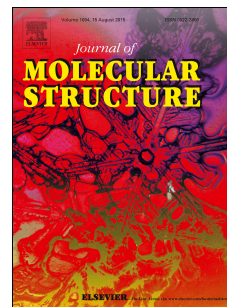


Accepted Manuscript

Optical, Fluorescence with Quantum analysis of Hydrazine (1, 3- Dinitro Phenyl) by DFT and Ab initio approach

D. Cecily. Mary Glory, K. Sambathkumar, R. Madivanane, G. Velmurugan, R. Gayathri, S. Nithiyantham, M. Venkatachalapathy, N. Rajkamal



PII: S0022-2860(17)31666-6

DOI: [10.1016/j.molstruc.2017.12.046](https://doi.org/10.1016/j.molstruc.2017.12.046)

Reference: MOLSTR 24665

To appear in: *Journal of Molecular Structure*

Please cite this article as: D. Cecily. Mary Glory, K. Sambathkumar, R. Madivanane, G. Velmurugan, R. Gayathri, S. Nithiyantham, M. Venkatachalapathy, N. Rajkamal, Optical, Fluorescence with Quantum analysis of Hydrazine (1, 3- Dinitro Phenyl) by DFT and Ab initio approach, *Journal of Molecular Structure* (2017), doi: 10.1016/j.molstruc.2017.12.046

This is a PDF file of an unedited manuscript that has been accepted for publication. As a service to our customers we are providing this early version of the manuscript. The manuscript will undergo copyediting, typesetting, and review of the resulting proof before it is published in its final form. Please note that during the production process errors may be discovered which could affect the content, and all legal disclaimers that apply to the journal pertain.

Highlights

- Hydrazine (1, 3- Dinitro Phenyl) crystal
- Optical, Fluorescence studies, Molecular structure – XRD,
- FTIR, FT-Raman, UV – stretching and opticals.
- Vibrations – HOMO-LUMO, SQMFF, NMR, MESP calculations.
- DFT, Ab initio calculation,

Fig caption

Figure 1. Cleaved Crystal of Hydrazine (1, 3- Dinitrophenyl).

Figure 2. Powder XRD of Hydrazine (1, 3- Dinitrophenyl).

Figure 3. High-resolution X-ray diffraction curve of Hydrazine (1, 3- Dinitrophenyl).

Figure 4. Emission spectrum of Hydrazine (1, 3- Dinitrophenyl).

Figure 5. Molecular structure of Hydrazine (1, 3- Dinitrophenyl).

Figure 6. Various conformers of Hydrazine (1, 3- Dinitrophenyl).

Figure 7. Comparison of observed and calculated IR spectra of Hydrazine (1, 3- Dinitrophenyl) (a) observed in solid phase (b) calculated with B3LYP/6-311+G(d,p) and (c) calculated with B3LYP/6-311++G(d,p) level.

Figure 8. Comparison of observed and calculated Raman spectra of Hydrazine (1, 3- Dinitrophenyl) (a) observed in solid phase (b) calculated with B3LYP / 6 -311+G(d,p) and (c)calculated with B3LYP/6-311++G(d,p) level.

Figure 9. Frontier orbital energy of Hydrazine (1, 3- Dinitrophenyl).

Figure 10. Experimental NMR spectrum of Hydrazine (1, 3- Dinitrophenyl).

Figure 11. UV spectrum of Hydrazine (1, 3- Dinitrophenyl).

Figure 12. The total electron density surface of Hydrazine (1, 3- Dinitrophenyl).

Figure 13. The contour map of electrostatic potential surface of Hydrazine (1, 3- Dinitrophenyl).

Figure 14. The molecular electrostatic potential surface of Hydrazine (1, 3- Dinitrophenyl).

Figure 15. Correlation graphic of thermodynamic parameters and Temperature for entropy (S), heat capacity at constant pressure (Cp), Gibb's free energy(G) energy change of Hydrazine (1, 3- Dinitrophenyl).

Figure 16. Correlation graphic of condensed fukui function of Hydrazine (1, 3- Dinitrophenyl).

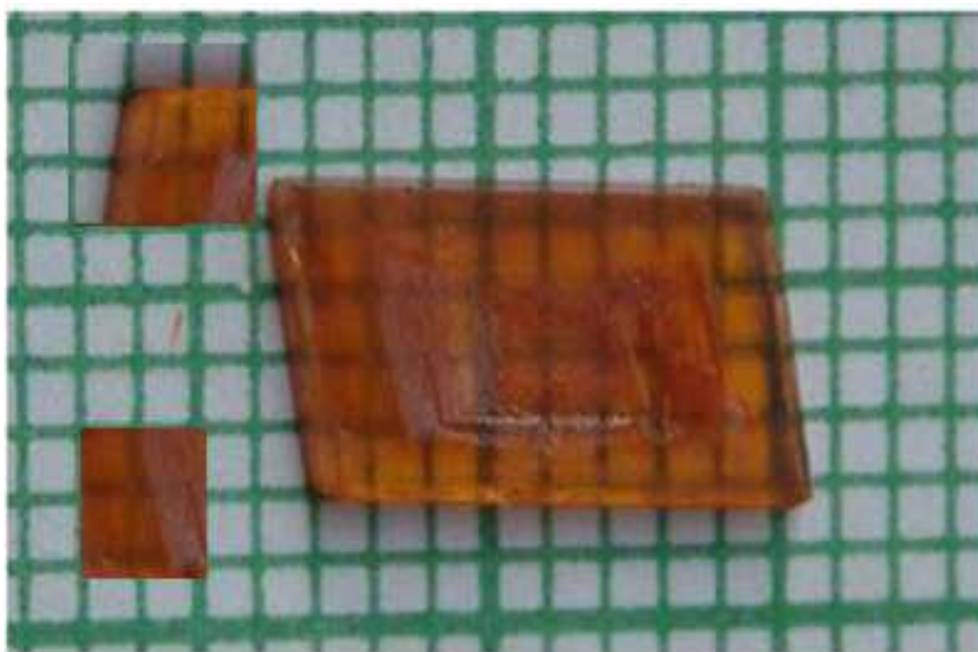


Figure..1.

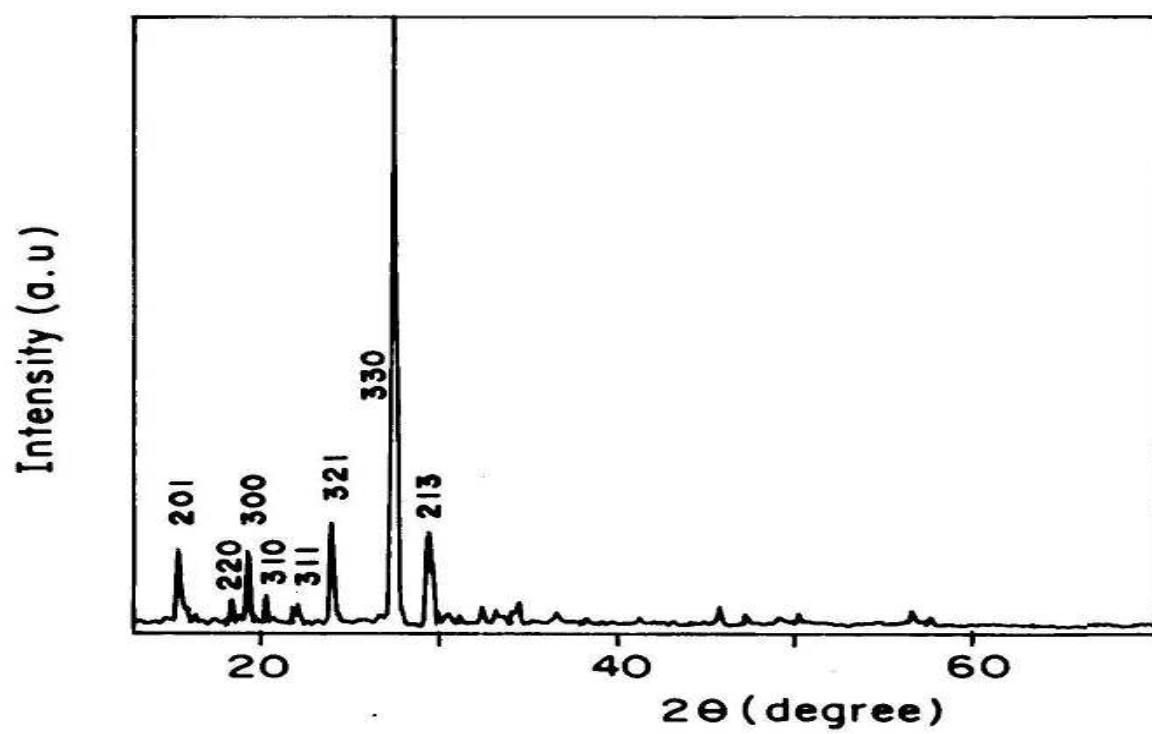


Figure..2.

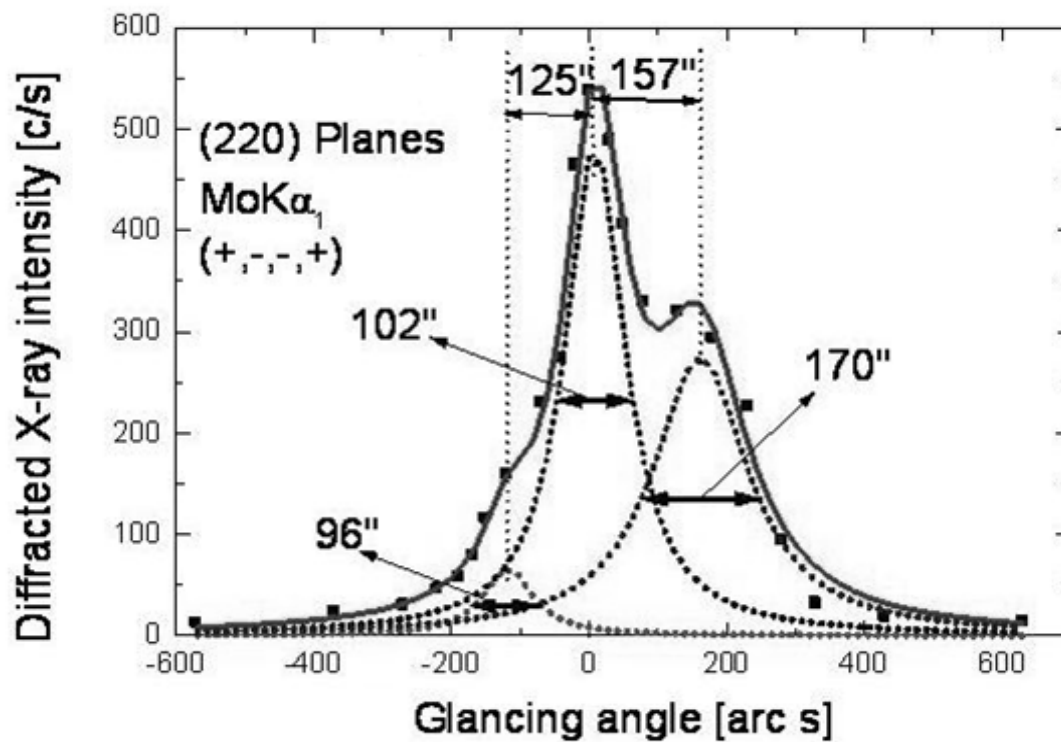


Figure.3.

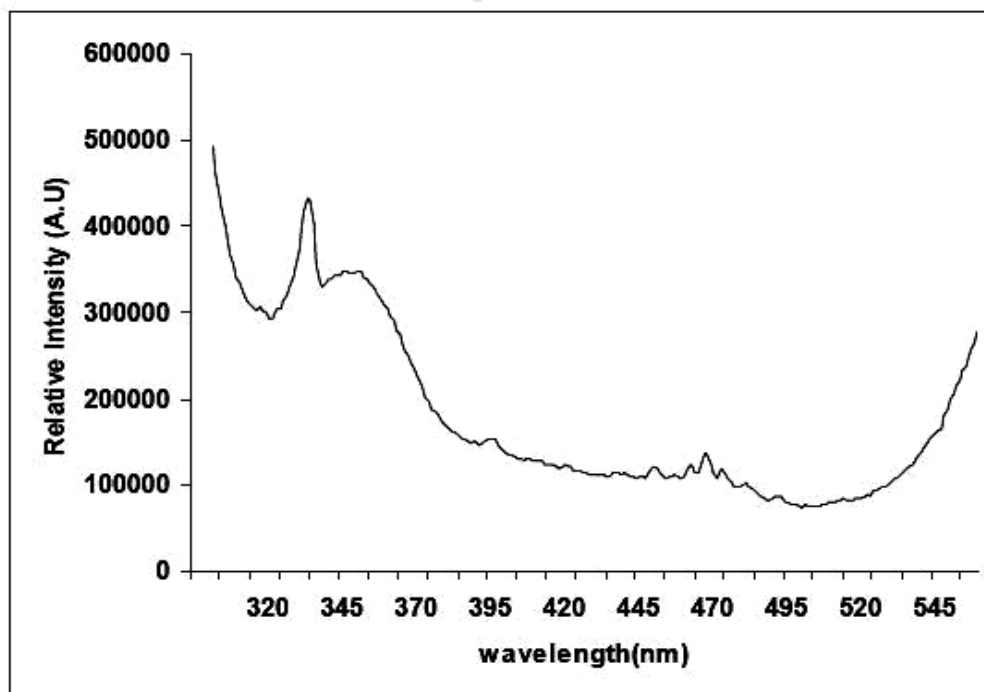


Figure .4.

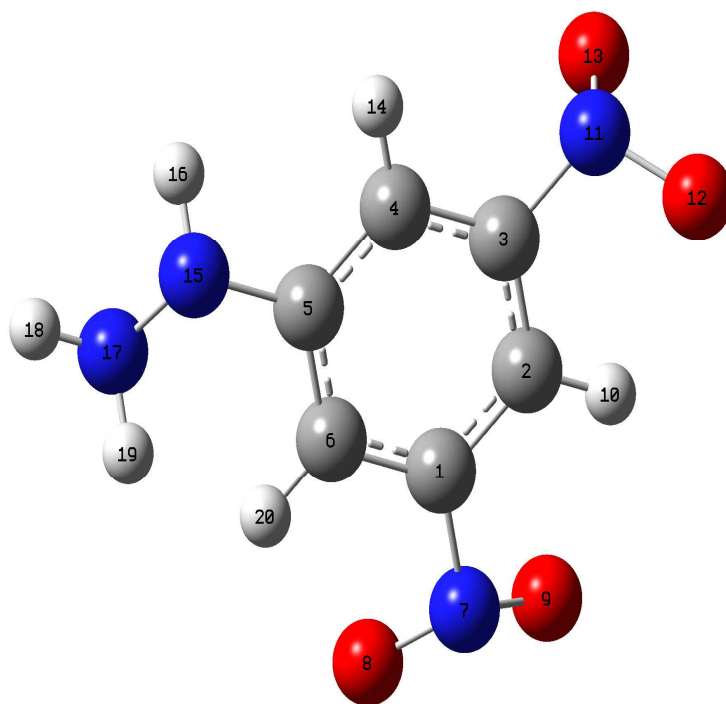


Figure .5.

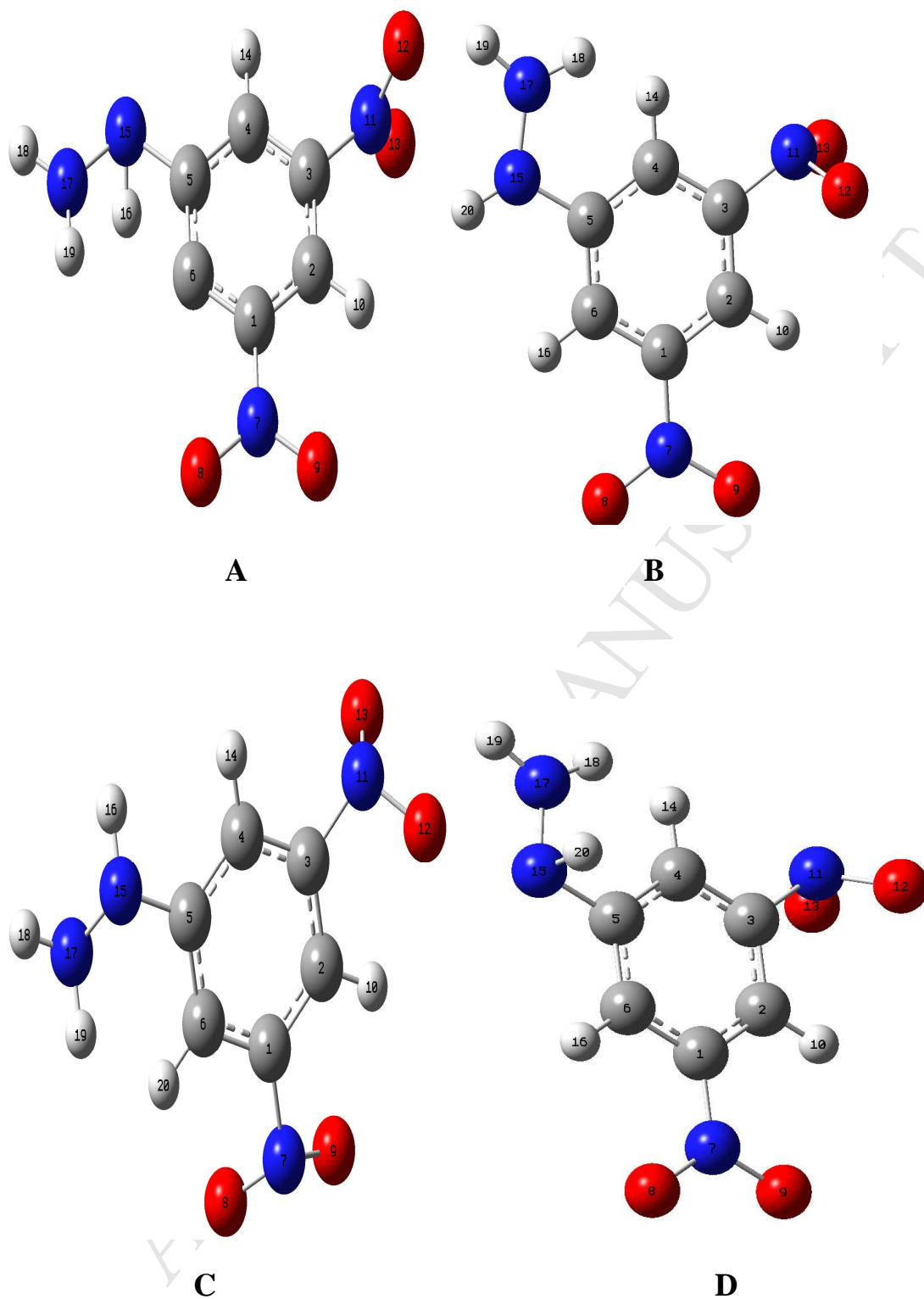


Figure 6.

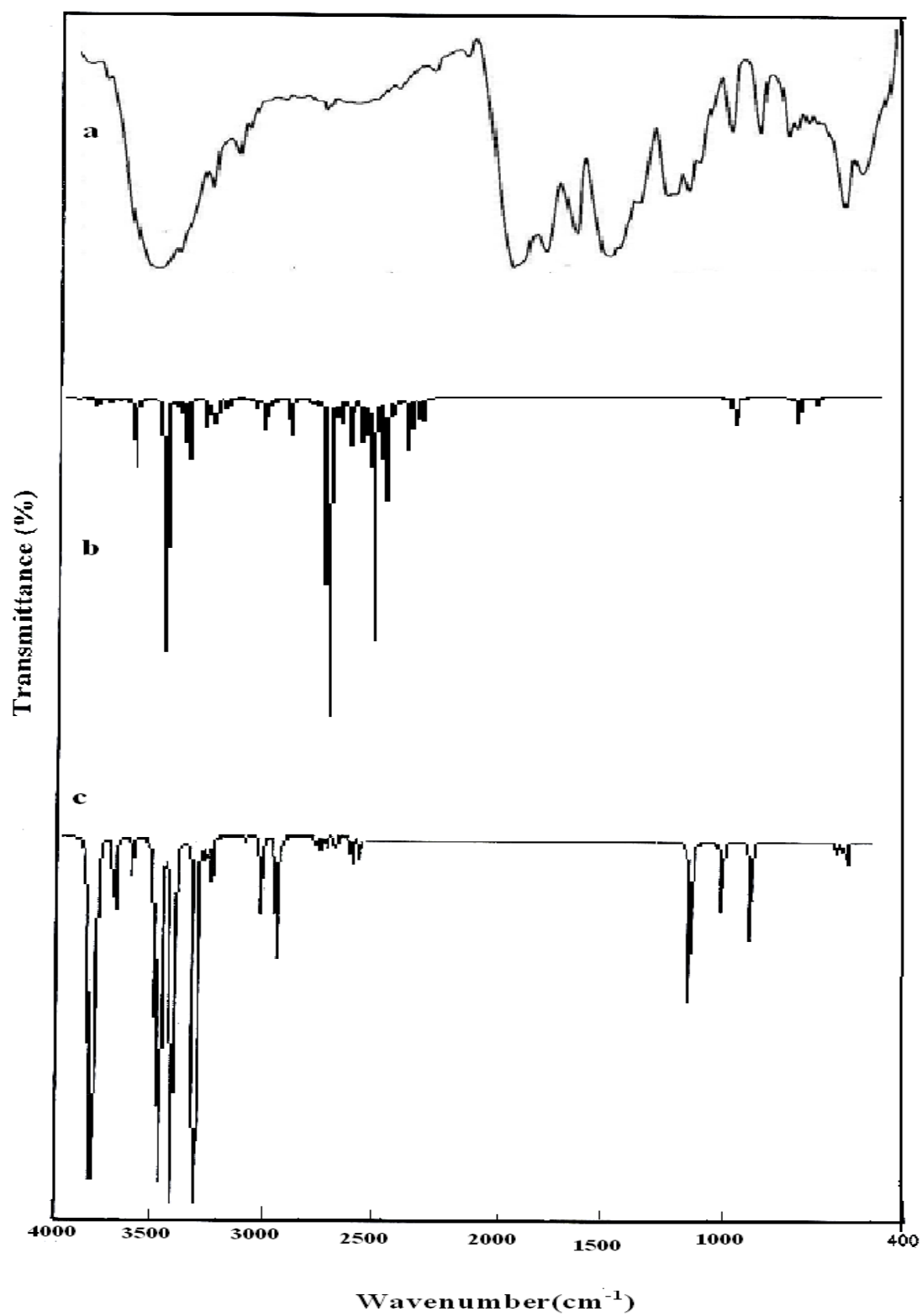


Figure.7

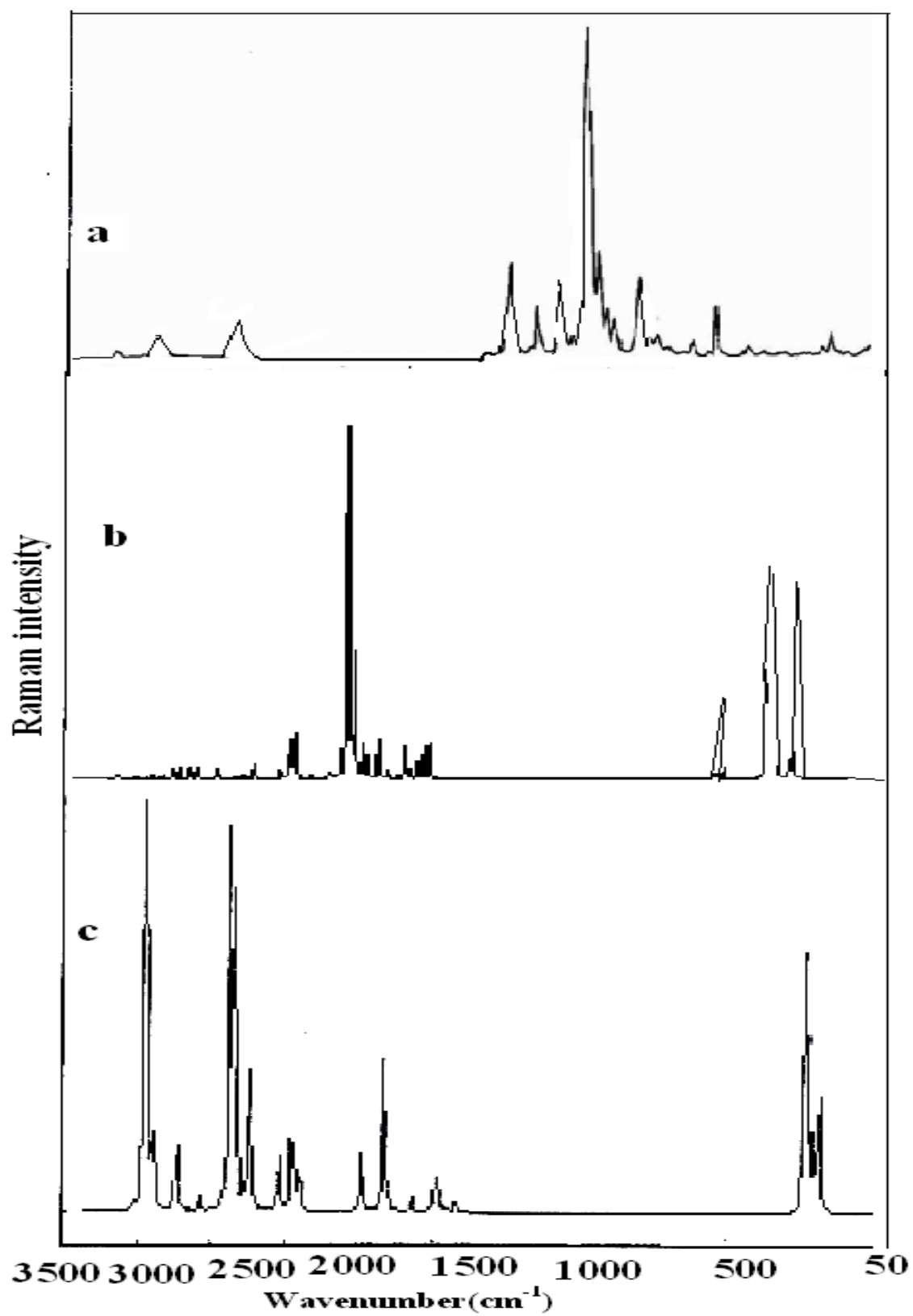


Figure. 8.

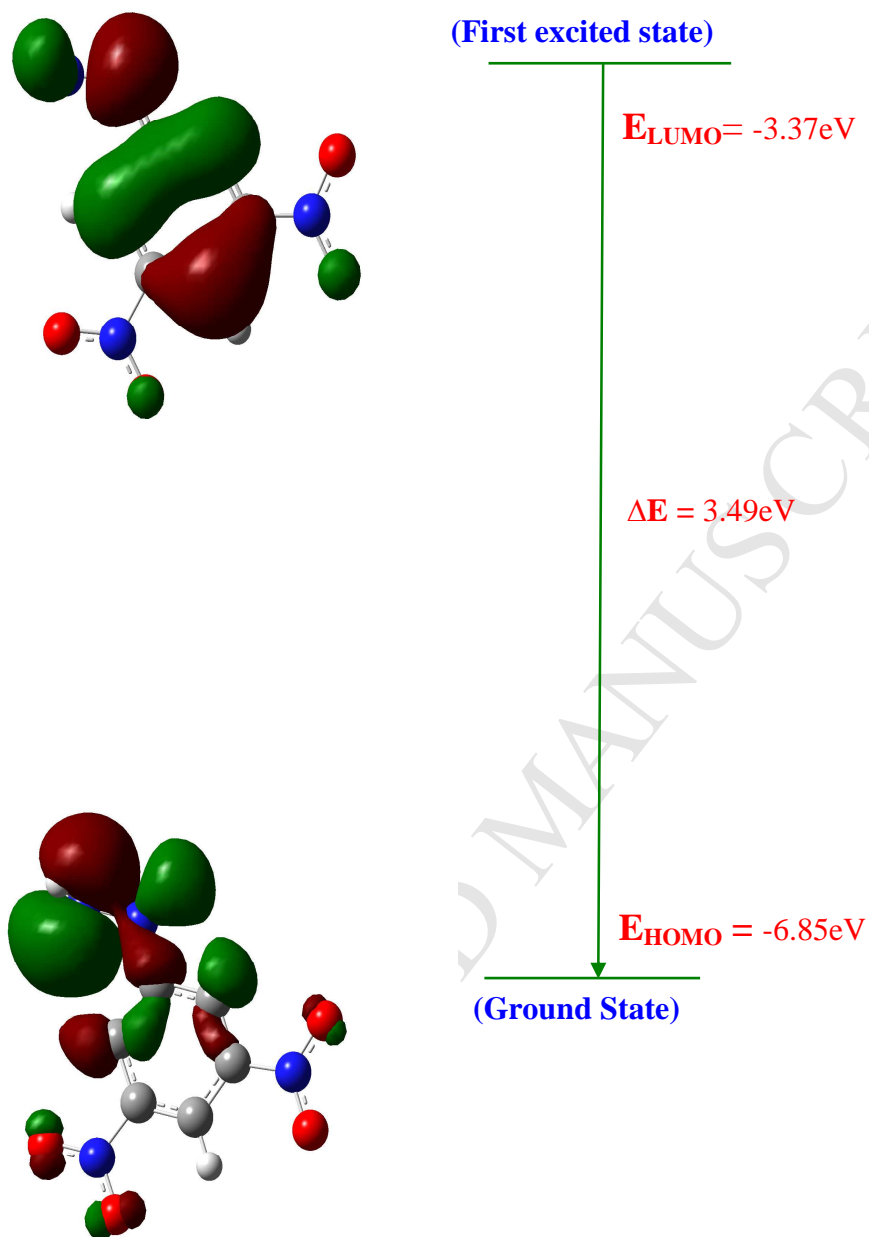


Figure.9.

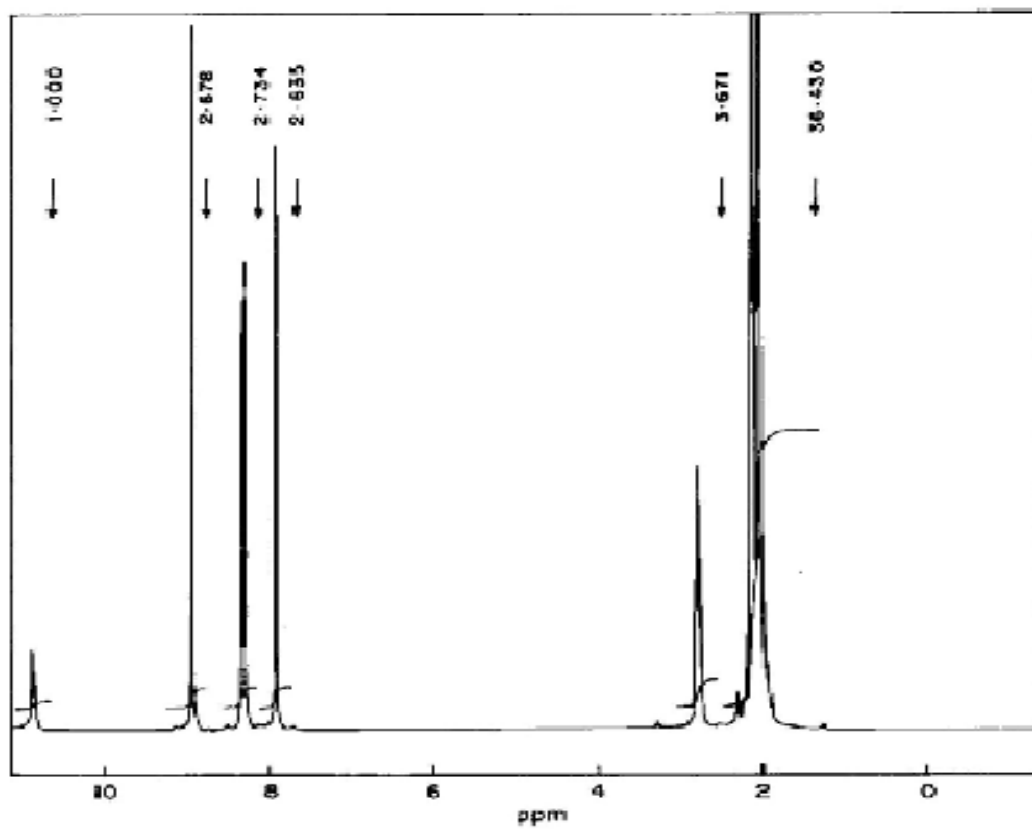


Figure. 10.

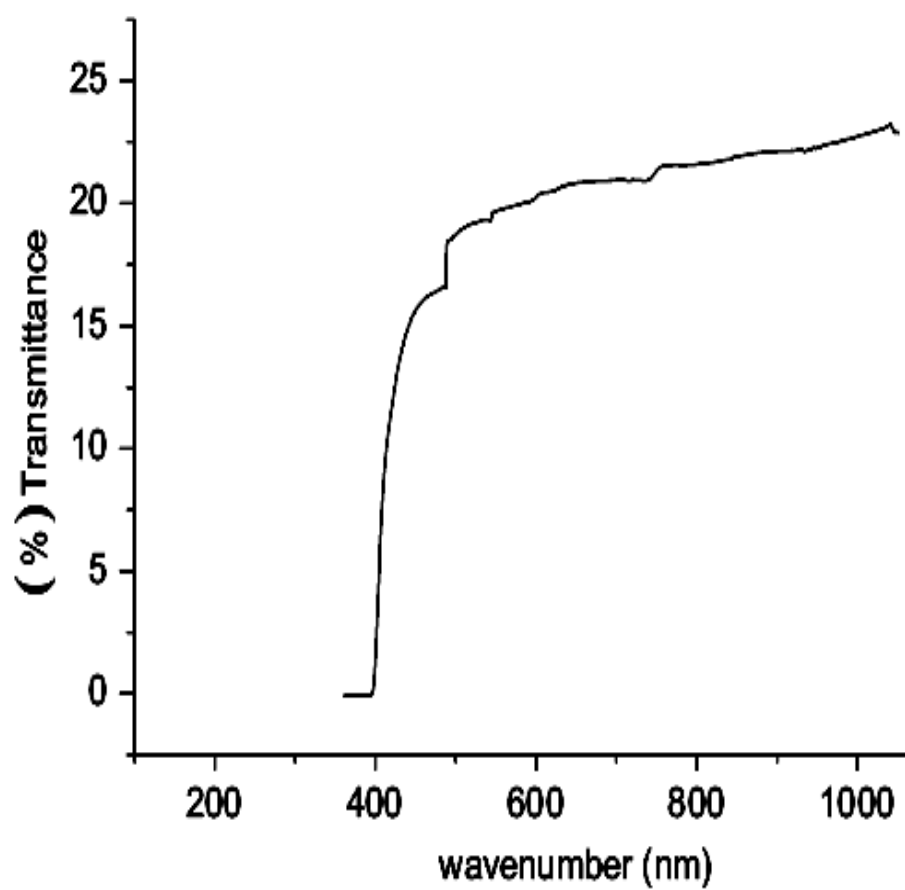


Figure .11.

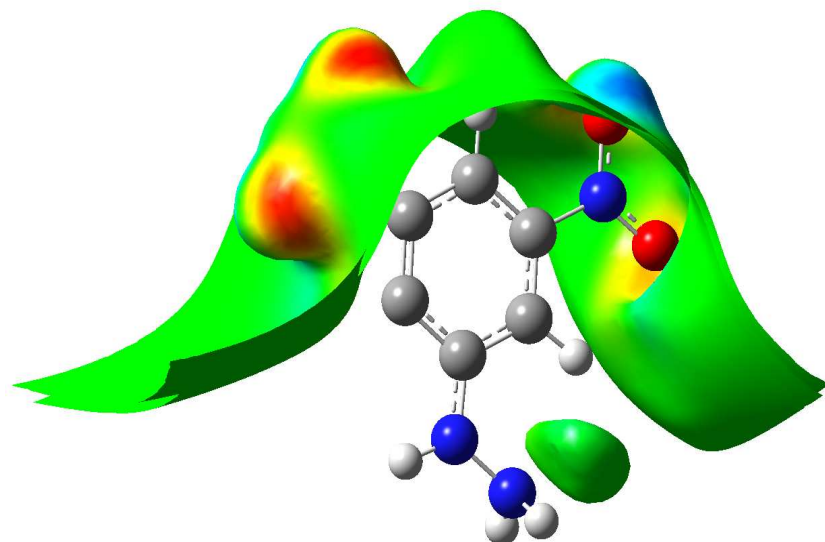


Figure. 12.

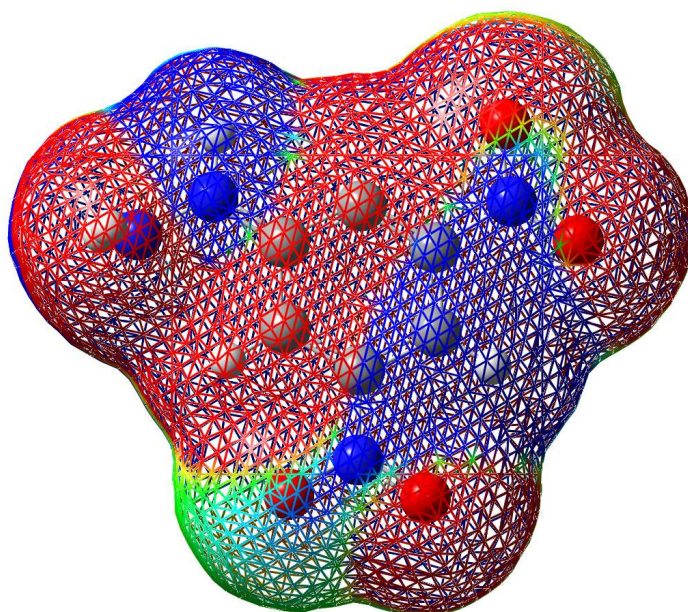


Figure. 13.

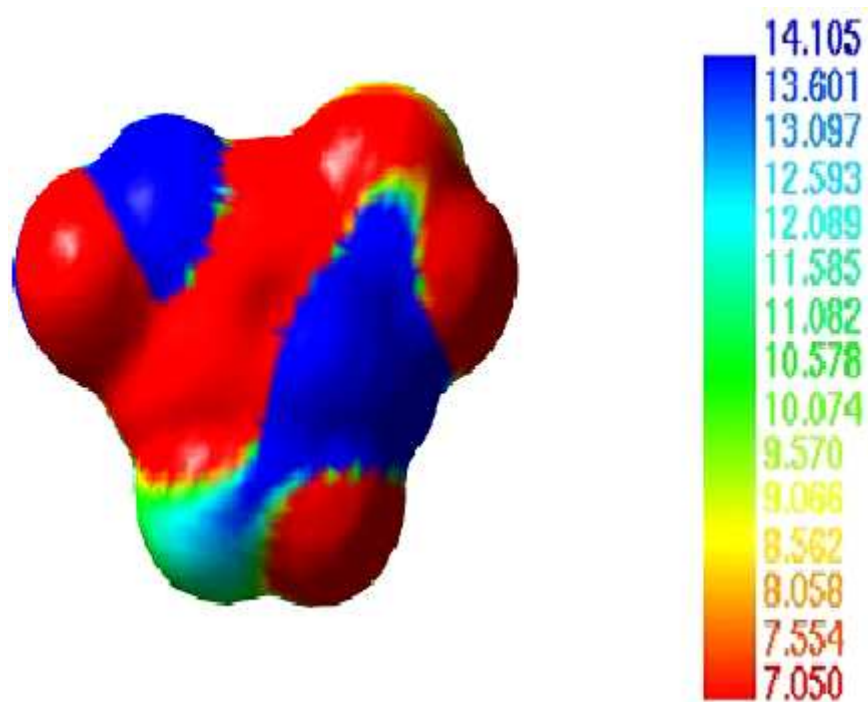


Figure. 14.

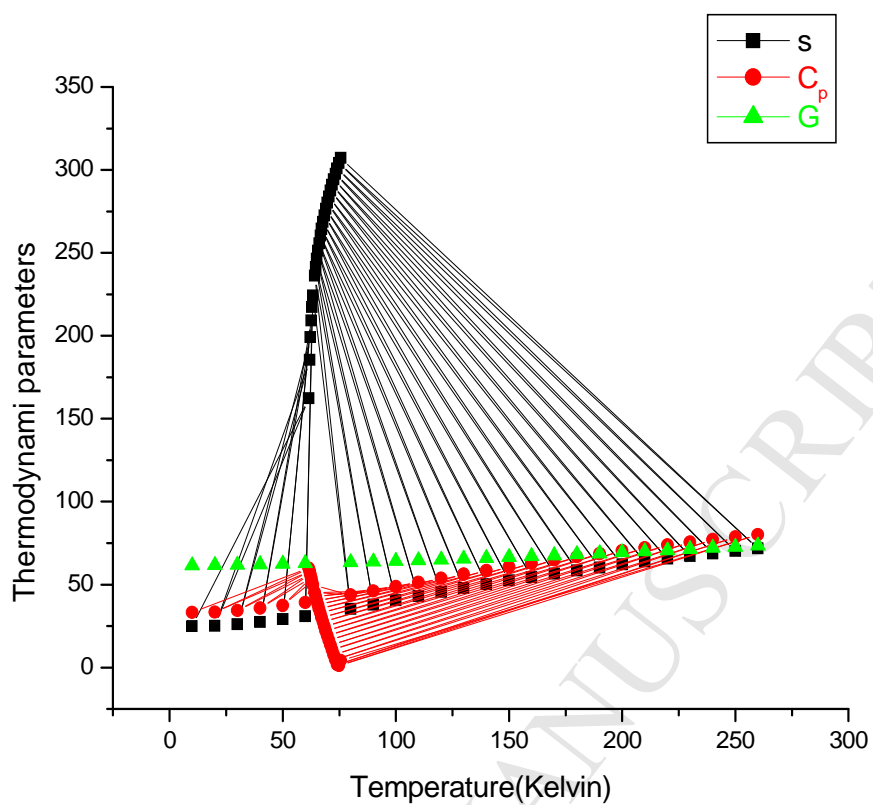


Figure .15.

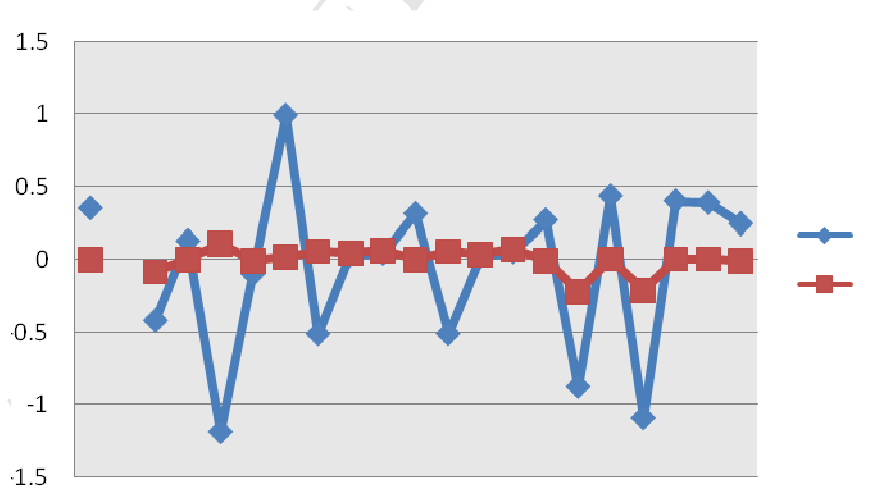


Figure. 16.

Optical, Fluorescence with Quantum analysis of Hydrazine (1, 3- Dinitro Phenyl) by DFT and Ab initio approach

^{1,2}D. Cecily. Mary Glory, ^{2,3}K. Sambathkumar ⁴R. Madivanane, ⁵G. Velmurugan,
⁶R. Gayathri ⁷S. Nithiyantham, ⁸M.Venkatachalapathy, ⁸N.Rajkamal

¹Research and Development Centre, Bharathiar University. Coimbatore, India-641046.

²Idhaya College of Arts and Science for Women, Puducherry, India-605008.

³PG.& Research Department of Physics, (Crystal growth centre), A.A.Govt.Arts College, Villupuram, Tamilnadu, India- 605602.

⁴Department of Physics, Mahatma Govt. College, Maye, Puducherry, India- 673311.

⁵Department of Chemistry, Indian Institute of Technology Bombay, Mumbai, India-400076.

⁶Department of Physics, Cauvery College for Women, Tiruchirappalli, India- 620018.

⁷Post Graduate and Research Department of Physics, (Solid state devices and Thin film laboratory Divisions), Thiru. Vi. Kalyanasundaram Govt Arts and Science College, Thiruvaur, Tamilnadu, India - 610003. (Affiliated to Bharathidasan University, Thiruchirappalli)

⁸PG & Research Department of Physics, Thiru.A.Govindasamy Govt Arts College, Tindivanam, Tamilnadu, India – 604002.

Corresponding author : s_nithu59@rediffmail.com

Contact: +91 9840980869

Abstract

Experimental and computational study of molecular structure, vibrational and UV-spectral analysis of Hydrazine (1, 3- Dinitrophenyl) (HDP) derivatives. The crystal was grown by slow cooling method and the crystalline perfection of single crystals was evaluated by high resolution X-ray diffractometry (HRXRD) using a multicrystal X-ray diffractometer. Fluorescence, FT-IR and FT-Raman spectra of HDP crystal were recorded. The assignments of the vibrational spectra

have been carried out with the help of normal co-ordinate analysis (NCA) followed by scaled quantum force field methodology (SQMFF). NMR studies have confirmed respectively the crystal structure and functional groups of the grown crystal. The energy and oscillator strength calculated by Time-Dependent Density Functional Theory (TD-DFT) result complements the experimental findings. The calculated MESP, UV, HOMO-LUMO energies show that charge transfer done within the molecule. And various thermodynamic parameters are studied. Fukui determines the local reactive site of electrophilic, nucleophilic, descriptor.

Key words: HDP, HRXRD, DFT, FMO Analysis, NMR.

1. Introduction

Hydrazones and hydrazides compounds are well known to possess various kinds of biological activities [1]. Hydrazone derivatives are used as fungicides, and in the treatment of diseases such as tuberculosis, leprosy and mental disorders etc. The complexes of various hydrazones and hydrazide are reported to act inhibitors of enzymes [2]. Many substituted hydrazides and hydrazones are employed in the treatment of psychotic and psychoneurotic conditions. Carboxylic acid hydrazones are known to exhibit strong antibacterial activities which are enhanced by complexation with metal ions. The study of biological activity on Hydrazine (1,3-dinitrophenyl) (HDP) proved that HDP is an important material for biological applications. Dinitrophenyl hydrazine is the constituents in various biomedical, pharmaceutical and related products and etc., [3, 4]. To our knowledge, the vibrational spectra and the theoretical calculations of Hydrazine (1,3-dinitrophenyl) have not been reported so far. In the present work the FT-IR, FT-Raman and UV-Visible-NIR spectral analysis were used. Quantum chemical computations have been recently used as an effective tool in the vibrational analysis of drug molecules, biological compounds and natural products, whereas substituted benzene derivatives

with high optical non-linearity are very promising materials for future optoelectronics and non-linear optical applications. Synthesis and grown crystal give Non-linear optical effects of compound depend on the polarizability of organic material are generally contribution from the lattice components because of the weak intermolecular bonding and hence possesses the high degree of delocalization. Single crystal X-ray diffraction study shows that HDP crystallizes in a monoclinic system. By combining all these facts, the present study has been aimed, to investigate the vibrational spectra of hydrazine (1,3- dinitrophenyl)(HDP) [5 - 9].

Investigations have also been carried out to identify the HOMO-LUMO energy gap, NLO property of first hyperpolarizability, chemical hardness, chemical potential and delocalization activity of the electron clouds in the optimized molecular structure. So, in this work, the vibrational wave numbers, geometrical parameters, modes of vibrations, minimum energy, proton NMR chemical shifts are calculated. Theoretical studies of bioactive compounds are of interest in order to gain a deeper insight on their action and thus helping in the design of new compounds with therapeutic effects. The knowledge of physico-chemical properties and sites of reaction of title compound will provide a deeper insight of its probable action. Particularly, molecular electrostatic potential is related to the electronic density and is a very useful descriptor in understanding sites for electrophilic attack and nucleophilic reactions as well as hydrogen bonding interactions. The calculated value of molecular and electronic properties is used to interpret the biological activity of the molecule [10-12].

2. Experimental procedure

Synthesis and crystal growth

In this experiment, about 85gm (866 mmol) of potassium acetate is added with 35gm (355.3 mmol) of hydrazine sulfate dissolved in 125ml of hot water in a 400ml beaker with constant stirring. The mixture is boiled for 5 minutes and then cooled to about 70° C. To this

75ml of alcohol is added and the generated solid is filtered and washed with 75ml of hot alcohol. The filtered hydrazine solution is used for the next step. To this hydrazine solution about 50.5gm (512.6 mmol) of 1,3-Dinitrochloro benzene is dissolved in 250 ml of alcohol is added and the mixture is refluxed with stirring for an hour in a flask fitted with stirring and reflux condenser. In the first ten minutes most of the product separates out. It is then cooled, filtered and washed with 50ml of hot alcohol to remove unchanged halide and then with 50ml of hot water. The pure solid weighs 30gm (304.5mmol) and melts at 190–192° C with evolution of gas. About total yield of 40-42 gm less pure second crop is obtained by distilling half the alcohol from the filtrate and recrystallized 30ml of from *n*-butyl alcohol. Alternatively 70% yield of hydrazine (dinitrophenyl) is obtained by substituting 10gm of NaOH for every 35gm of potassium acetate by boiling for five minutes without filtering the salt. Crystals were grown by the slow cooling method by reducing the temperature from 30°C at the rate of 0.1°C per day. The two important factors influence the habit of growing crystal, (i) the polarity of the solvents and stirring the solution. (ii) Solvent offering moderate solubility temperature gradient to yield prismatic growth [5-7].

Forming of Single crystal dimension is 8 x 4 x 2 mm³ was grown (Fig. 1) in a period of 7 days. All chemical obtain from the Lancaster chemical company, UK, the chemicals were of reagent grade and used as commercially purchased without additional purification. All solvents were dried and distilled before use.

3. Characterization Techniques

Single-crystal X-ray diffraction analysis of HDP was carried out using ENRAF NONIUS CAD-4 diffractometer with Mo K α (0.71073 Å) radiation. A PANalytical X'Pert PRO MRD high-resolution XRD system, with Cu K α_1 radiation, was employed to assess the crystalline

perfection of grown crystals. The rocking curves of the crystals for the (200) diffraction planes were recorded in symmetrical Bragg geometry using the (100) natural facets by performing an ω scan with triple-axis geometry. The monochromated X-ray beam incident on the specimen was obtained using a hybrid two-bounce Ge (220) monochromator with a parabolic multilayer mirror assembly. The diffracted beam from the specimen was detected using a scintillation detector with a triple-axis three bounce Ge(220) analyzer. FTIR and FT-Raman spectrum were recorded using the Perkin Elmer spectrum one FTIR spectrometer by KBr pellet technique and Bruker RFS 27 in the region 4000–400 cm^{-1} . The NMR spectra recorded using JEOL GSX 400 model at 23 °C. The experiment was carried out in the frequency range 100 Hz–5 MHz at room temperature. The grown crystals were tested for their micro hardness property using Shimadzu HMV Vickers's micro hardness tester fitted with diamond indenter. UV spectrum was recorded using Shimadzu model 1601 in the range of 300 – 1000 nm.

3.1. X-Ray Diffraction analysis

Single crystal X-ray diffraction studies Single crystal X-ray diffraction analysis of the grown HDP crystal has been carried out to confirm the crystallinity and also to identify the unit cell parameters. HDP exhibited as a monoclinic structure with space group of P21/c. Also, the powder XRD pattern recorded are indexed and shown in Fig 2. The lattice parameters were calculated from single crystal data and the calculated values are given in Table 1 and the final atomic coordinates are listed in Table 2 with values reported in the literature for the sake of comparison. The results are in agreement with the earlier reported values [8].

3.2. High Resolution X-Ray Diffraction

Before recording the diffraction curve to remove the non-crystallized solute atoms remained on the surface of the HDP crystal and also to ensure the surface planarity, the specimen

was first lapped and chemically etched in a non-preferential etchant of acetone and water mixture in 2: 1 volume ratio. Fig 3 shows the high-resolution diffraction curve (DC). The solid line (convoluted curve) is well fitted with the experimental points represented by the filled rectangles. On deconvolution of the diffraction curve, it is clear that the curve contains two additional peaks, which are 125 and 157 arc away from the main peak. These two additional peaks correspond to two internal structural low angle (tilt angle ≥ 1 arc min but less than a degree) boundaries [9] whose tilt angles (misorientation angle between the two crystalline regions on both sides of the structural grain boundary) are 125 and 157 arc sec from their adjoining regions. The FWHM (full width at half maximum) of the main peak and the low angle boundaries are respectively 102, 96 and 170 arc sec. Though the specimen contains low angle boundaries, the relatively low angular spread of around 10 arc min of the diffraction curve and the low FWHM values show that the crystalline perfection is reasonably good. The effect of such low angle boundaries may not be very significant in many applications, but for the phase matching applications, it is better to know these minute details regarding crystalline perfection [10].

3.3. Fluorescence Studies

Fluorescence may be expected generally in molecules that are aromatic or contain multiple conjugated double bonds with a high degree of resonance stability [11]. Fluorescence finds wide application in the branches of biochemical, medical, and chemical research fields, for analyzing organic compounds. It is also used as lighting of fluorescent lamps, LED etc. The emission spectrum for HDP was recorded using FP-6500 Spectrofluorometer in the range 320 – 520 nm (Fig. 4). It is observed that the compound was excited at 320 nm. The emission spectrum shows a sharp peak at 335 nm due to $\pi - \pi^*$ transition, and broad peaks at 398 nm is due to $n - \pi^*$ transition.

3.4. Computational Methodology

Initial geometry of HDP was optimized using the B3LYP method using of GAUSSIAN 09W package [12]. The vibrational frequency analysis was computed using B3LYP/6-311++G(d,p) level of theory to determine the nature of a stationary point found by geometry optimization. The hyperpolarizability and the chemical shift of the atoms of HDP have been calculated using B3LYP/6-311++G(d,p) level of theory. The frontier molecular analysis has been carried out to explain the charge transfer within the compound. The chemical hardness (η) and chemical potential (μ) have been calculated. The comparison between the calculated and the observed vibrational spectra helps us to understand the observed spectral features. In order to improve the agreement of calculated frequencies with experimentally calculated frequencies, it is necessary to scale down the theoretically calculated harmonic frequencies. Hence, the vibrational frequencies theoretically calculated at B3LYP/6-311++G(d,p) and 6-311++G(d,p) are scaled down by using MOLVIB 7.0 version written by Tom Sundius [13,14]. The Raman activities (S_i) calculated by GAUSSIAN 09W package have been suitably adjusted by the scaling procedure with MOLVIB and subsequently converted to relative Raman intensities (I_i) using the following relationship derived from the basic theory of Raman scattering [15-17].

$$I_i = \frac{f(v_o - v_i)^4 S_i}{v_i [1 - \exp(-\frac{hc v_i}{kT})]} \quad (1)$$

where v_o is the exciting frequency (cm^{-1} units). v_i is the vibrational wave number of the i^{th} normal mode, h , c and k are universal constants for cell parameter, and f is the suitably chosen common scaling factor for all peak intensities.

4. Results and Discussion

4.1. Optimized Geometry

The optimized molecular structure and numbering scheme of HDP are represented in Fig 5. The geometry of the compound under investigation is considered by possessing C_1 point group

symmetry. The geometrical parameters of the title compound are given in Table 3. Detailed description of vibrational modes can be given by means of normal coordinate analysis. The internal coordinates describe the position of the atoms in terms of distances, and dihedral angles with respect to an origin atom. The symmetry coordinates are constructed using the set of internal coordinates. This study explains the full set of 66 standard internal coordinates (containing 12 redundancies) for HDP (Table 4). From these, a non-redundant set of local symmetry coordinates were constructed by suitable linear combinations of internal coordinates following the recommendations of Fogarasi *et al* [18,19] are summarized in Table 5. In order to find the most optimized geometry, the energy calculations are carried out for various possible conformers. The various possible conformers of HDP are shown in Fig 6. In Figure 6 (B) is the molecule structure of HDP. For the molecules, the global minimum energy calculations are carried out for four different possible conformers. The (*) represents global minimum energies obtained for these conformers are listed in Tables. 6. The most stable structure obtained for the HDP via B3LYP/6-311++G(d,p) level. To check whether the chosen set of symmetric coordinates contribute maximum to the potential energy associated with the molecule, the TED has been carried out.

4.2. Vibrational Frequency Analysis

The title compound consists of 20 atoms and its 54 normal modes distributed amongst the symmetry spaces as

$$\overline{3N-6} = 37 A' (\text{in - plane}) + 17 A'' (\text{out-of-plane}) \quad (2)$$

All the vibrational assignments of the 54 fundamentals of HDP along with the experimentally and theoretically calculated IR, Raman frequencies, IR intensities, Raman activities, and force constants are presented in Table 7. The FT-IR and FT-Raman spectra of the title compound are

shown in (Figs.7-8), respectively. Since the identification of all normal modes of vibration of compounds is not trivial, we tried to simplify the problem by considering each compound as substituted benzene. Such an idea has already been successfully utilized by several workers for vibrational assignment of compounds containing multiple Homo-Lumo and aromatic rings [4].

4.2.1. N-H Vibrations

The hetero aromatic molecule containing an N-H group shows its stretching absorption in the region 3500–3220 cm^{-1} . The position of absorption in this region depends upon the degree of hydrogen bonding, and hence upon the physical state of the sample or the polarity of the solvent. The vibrational bands due to the N-H stretching are sharper and weaker than those of NH_2 stretching vibrations by virtue of which they can be easily identified [20]. In our present study the very weak band observed in FT Raman spectrum at 3176 cm^{-1} are assigned to N-H stretching vibration. The theoretically computed wave numbers by B3LYP/6-311++G(d,p) method at 3175 cm^{-1} is attributed to N-H stretching vibration. The in-plane and out-of-plane bending vibration of N-H group are also supported by the literature [21].

4.2.2. C-C Vibrations

The benzene possesses six stretching vibrations of which the four with highest wave numbers occurring near 1650-1400 cm^{-1} are good group vibrations [21]. With heavy substituents, the bands tend to shift to somewhat lower wavenumbers and greater the number of substituents on the ring, broader the absorption regions. As predicted in the earlier references, in this present investigation, the C-C stretching (weak- very weak) vibrations observed at 1699, 1687, 1664, 1651 cm^{-1} in FT-IR and 1679, 1670 cm^{-1} very weak band observed in FT-Raman spectrum for HDP. The theoretically computed wave number by B3LYP/6-311++G(d,p) level at 1795-1687

cm^{-1} is attributed to C–H stretching vibration. The C–C in-plane and out-of-plane bending modes of HDP are summarized in Table 7.

4.2.3. C–N Vibrations

The C–N stretching frequencies in the side chain are a rather difficult task, since there are problems in identifying these frequencies from other vibrations. The C–N stretching usually lies in the region $1400\text{--}1200\text{ cm}^{-1}$, since, mixing of bands is possible in this region [21]. However, with the help of force field calculations, the C–N vibrations are identified for the title compound. In this study, the C–N stretching (very strong – strong) vibrations of HDP are found at 1589 cm^{-1} in the FT-IR spectra and at $1593, 1574\text{ cm}^{-1}$ in the FT-Raman spectrum. The theoretically computed wave number by B3LYP/6-311++G(d,p) method at $1595\text{--}1575\text{ cm}^{-1}$ is attributed to C–N stretching vibration. The C–N bending vibrations and deformations are in close agreement with literature values.

4.2.4. C–H Vibrations

The aromatic compounds commonly exhibit multiple bands in the region $3100\text{--}3000\text{ cm}^{-1}$ due to C–H stretching vibrations. In this molecule, the strong to medium strong bands are observed at $3144, 3098$ and 3077 cm^{-1} assigned to C–H ring stretching vibrations. The theoretically computed wave number by B3LYP/6-311++G(d,p) level at $3142\text{--}3078\text{ cm}^{-1}$ is attributed to C–H stretching vibration. Here, the IR bands are strong, whereas the Raman bands are weak. The C–H in plane ring bending vibrations normally occurred as a number of strong to weak intensity sharp bands in the region $1300\text{--}1000\text{ cm}^{-1}$ [21]. The bands for C–H in plane bending vibrations are identified at 1392 cm^{-1} for FT-IR spectrum and at $1496, 1373\text{ cm}^{-1}$ in the FT-Raman spectrum. The C–H out of plane bending vibrations is normally observed in the region

950-809 cm^{-1} . In the present case, the C-H out of plane bending bands is observed at 1003, 975 and 991 cm^{-1} . Like in plane bending, all the strong to weak bands were observed in FT-IR and Raman spectrum. The assigned frequencies for C-H vibrations are found to be well within their characteristic regions and it is infer that, C-H vibrations have not affected by the substitutions.

4.2.5. NO_2 Vibrations

There are six normal modes due to an NO_2 group namely asymmetric NO_2 stretching, symmetric NO_2 stretching, NO_2 rocking, NO_2 wagging and NO_2 torsion. The NO_2 asymmetric stretching vibration band range is 1625 - 1540 cm^{-1} and that of symmetric stretching vibration is 1400 - 1360 cm^{-1} [22]. Here, the very weak NO_2 asymmetric stretching vibrations for both IR spectra are observed at 1646 and 1635 cm^{-1} . The weak to very weak symmetric stretching vibration is observed at 1619 and 1610 cm^{-1} in FTIR spectrum for HDP. The theoretically computed wave number by B3LYP/6-311++G(d,p) level at 1642-1613 cm^{-1} is attributed to NO_2 (asymmetric and symmetric) stretching vibration.. The weak NO_2 scissoring vibration is observed at 931 cm^{-1} in IR spectrum and at 927 cm^{-1} in the FT-Raman spectrum. The deformation vibrations of NO_2 group (rocking, wagging and twisting) contribute to several normal modes in the low frequency region. These bands are also found well within the characteristic region and are presented in Table 7.

4.2.6. NH_2 Vibrations

The molecule of HDP under consideration possesses NH_2 group in the fifth position of the heterocyclic ring. The NH_2 group gives rise to six internal modes of vibrations viz., the symmetric stretching, the anti symmetric stretching, the symmetric deformation or the scissoring, the rocking, the wagging and torsional modes [23]. The NH_2 group has two NH stretching vibrations, one begging asymmetric and the other symmetric. The frequency of asymmetric

vibration is higher than that of symmetric one. In HDP the very weak to very strong bands observed at 3312 and 3228 cm^{-1} in the FT-IR are assigned to asymmetric and symmetric stretching vibration respectively. Based on the above conclusion, the theoretically scaled down wave number at 3313 and 3229 cm^{-1} B3LYP/6-311++G(d,p) method are assigned to NH_2 asymmetric and symmetric stretching vibrations respectively. In addition the NH_2 group has scissoring, rocking, wagging and torsion modes. The deformation vibration observed in the FT-IR spectrum as a weak band at 1628 cm^{-1} is assigned to NH_2 scissoring vibration. The theoretically scaled down values at 1629 cm^{-1} by B3LYP/6-311++G(d,p) level respectively assigned to NH_2 scissoring vibration. The scaled down wave number at 1279 cm^{-1} is assigned to NH_2 rocking vibration and this vibration is far below the recorded spectral range. The weak frequency in the FT-IR spectrum at 1212 cm^{-1} assigned to NH_2 wagging mode correlates with the frequencies 1213 cm^{-1} computed by the B3LYP/6-311++G(d,p) levels respectively. The NH_2 twisting vibration computed by B3LYP/6-311+G(d,p) level at 286 cm^{-1} shows good agreement with the recorded weak FT-Raman frequency of 284 cm^{-1} .

4.3. Prediction of First Hyperpolarizability (β)

The hyperpolarizability (β_0) of this novel molecular system and the related properties (β_0, α_0) of HDP are calculated using the B3LYP/6-311+G(d,p) and B3LYP/6-311++G(d,p) level, based on the finite field approach. In the presence of an applied electric field, the energy of a system is a function of the electric field. The hyperpolarizability is a third-rank tensor that can be described by a $3 \times 3 \times 3$ matrix. The 27 components of the 3D matrix can be reduced to 10 components due to the Kleinman symmetry [23]. It can be given in the lower tetrahedral. The components of β are defined as the coefficients in the Taylor series expansion of the energy in the external electric field. When the external electric field is weak and homogenous, this expansion becomes:

$$E = E_0 - \mu_\alpha F_\alpha - 1/2\alpha_{\alpha\beta} F_\alpha F_\beta - 1/6\beta_\alpha\beta_\gamma F_\alpha F_\beta F_\gamma + \dots \quad (3)$$

Where E_0 is the energy of the unperturbed molecules, F_α the field of the origin and μ_α , $\alpha_{\alpha\beta}$ and $\beta_\alpha\beta_\gamma$ are the components of dipole moment, polarizability and the first hyperpolarizabilities, respectively.

The total static dipole moment μ , the mean polarizability α_0 and the mean first hyperpolarizability β_0 , using the x, y, z components [12]

The β_0 components of GAUSSIAN 09W output are reported in atomic units and therefore the calculated values are converted into e.s.u. units (1 a.u. = 8.3693×10^{-33} e.s.u.). The calculated value of hyperpolarizability and polarizability of HDP are in Table 8.

4.4. Electric fields effects on Transport Properties

The spatial redistribution of the frontier orbital is a three dimensional representation of local density of states which visually shows the electron density of the molecule. The highest occupied molecular orbital (HOMO), the lowest unoccupied molecular orbital (LUMO) are the frontier orbital's, the difference between them are known as HOMO-LUMO gap (HLG). HLG is one of the key factors determining the transport properties of the molecule. Large decrease in the HLG predicts the possibility of having reasonable conduction through the molecule, since, the conductivity increases with decreases in HLG. As the field increases the HLG extensively decreases from which is calculated from Gaussian 09 programme package. Fig 9 illustrates the spatial redistribution of the molecular orbital of the molecule. Table 9, even though small HLG exists in this molecular system, the possibility of conduction through the molecules is found to be very less, therefore, it almost act as an insulator. The analysis of the wave function is mainly described by one-electron excitation from the highest occupied molecular orbital (HOMO) to the lowest unoccupied molecular orbital. The HOMO–LUMO analysis of these compound is done at

B3LYP/6-311++G(d,p) level of theory. Fig.5 illustrates the orbital distributions of HOMO and LUMO levels of the title compound. HOMO is delocalized mainly on ring carbons; the oxygen takes part in the formation of HOMO of HDP. Fig. 9 shows that there is no electronic projection in HOMO and LUMO over the ring hydrogen atoms of the compound [24].

4.4.1. Inhibition efficiency through back donations ($\Delta E_{\text{back-donation}}$)

The electronic back donations process might be occurring governing the interaction between the inhibitor molecule and the metal surface. The concept establishes that if both processes occur, namely charge transfer to the molecule and back-donation from the molecule, the energy change is directly proportional to the hardness of the molecule as indicated in following expression:

$$\Delta E_{\text{back-donation}} = -\eta/4 \quad (4)$$

The $\Delta E_{\text{back-donations}}$ suggest that when $\eta > 0$ and $\Delta E_{\text{back-donation}} < 0$ the charge transfer to a molecule is actively favored followed by a back – donation from the molecule. In this environment, it is possible to balance the stabilization among inhibiting molecules. The maximum charge transfer ΔN_{max} is also used to predicate the inhibitor efficiency. The values of ΔN_{max} indicate the trend within a set of molecules and the highest value of ΔN_{max} is related to high inhibitor efficiency. All the calculated ΔN_{max} and $\Delta E_{\text{back-donation}}$ of Rose and its derivatives are collected. In this study, the highest value of $\Delta E_{\text{back-donation}}$ is -0.2691 eV which is tabulated in Table 9.

4.5. NMR Spectral Analysis

^{13}C NMR chemical shift is one of the pioneer tools in determining the presence or the absence of a particular atom in a molecule. In a molecule, shielding of atoms is greatly affected by the neighbouring bonded atoms. Similar bonded atoms give different shielding values in different environments. In the present analysis, the chemical shift values for Carbon and Hydrogen atoms

were studied. The structural parameter for NMR calculation was taken from the optimized geometries at B3LYP/6-311+G(d,p) level of theory. All the calculations were performed using Gauss view molecular visualization program and GAUSSIAN 09W program package. ^{13}C and ^1H NMR spectra of the title molecule are shown in Fig 10. The result shows that the range ^{13}C NMR chemical shift of the typical organic molecule usually is >100 ppm, the accuracy ensures reliable interpretation of spectroscopic parameters. The values obtained for all the carbon atoms show similar range except few. It is reasonable to discuss those carbon atoms, which possess distinguished chemical shift values from the others. The few carbon atoms have the shift value in higher and lower range. This can be attributed to the bond formed with electronegative atom, which causes the transfer of electron cloud around electronegative atoms from carbon thus deshielding the carbon. The peculiar thing is to be noted that the functional groups have been greatly affected in NMR studies, and high shift values are found in the structure requiring low field for resonance. C1 atom is mostly localized on periphery of the molecules and their chemical shifts would be more susceptible to intermolecular interactions in the aqueous solutions as compared to other atoms. Aromatic carbons give signals in overlapped areas of the spectrum with chemical shift values from 100 to 150 ppm [25-27]. In this study, the theoretical chemical shift and experimental values of aromatic carbons except C1 of HDP are in the range of 82.734 -187.473 and 25.635 (H11) 22.678 (H15)ppm. The chemical shift of C1 and H11 (118.009 ppm and 21.66 ppm in gas phase values) values of carbons because of the substitution of H group in HDP. The theoretical C4 and H15 atoms are due to the presence of electronegative oxygen in the 'O' group. The theoretical chemical shift values of HDP are compared with experimental values. ^{17}O has a very wide chemical shift range which for small molecules partially compensates for its broad signals. The theoretical values of ^{17}O is ranging from - 40 to 1120 ppm [34]. In the title compound, the peaks at 137.53 and 141.11 ppm are assigned to O₉ and O₁₀ which is HDP oxygen of the compound. Noticeably, the oxygen

experimental of HDP is larger than other oxygen due to the environment. Chemical shift values are represented in Table 10.

4.6. UV-VIS Spectral analysis

The UV-Vis spectrum of the reaction medium at 3hours after diluting a 1ml of the sample into 4ml of distilled water. UV-Vis spectral analysis was done by using UV-VIS spectrophotometer. The electronic absorption corresponds to the transition from the ground to the first excited state and is mainly described by one electron excitation from the (HOMO) to (LUMO). Electronic transitions are usually classified according to the orbitals engaged or to specific parts of the molecule involved. Common types of electronic transitions in organic molecules are $\pi - \pi^*$, $n - \pi^*$ and $\pi^*(\text{acceptor}) - \pi(\text{donor})$. For HDP the UV-Vis absorption spectra have been studied and show three intense peaks of 329.77, 240.01 and 200.11 nm. The UV- visible spectra showed a strong Plasmon resonance that shown in Fig.11. The representative derivatives reveal a common low-energy broad band assigned to intramolecular electronic transfer (ET) band. These are evident from the following theory. It is known that the photon energy is given by equation:

$$E = hc / \lambda \quad (5)$$

Where h - is the Planck's constant, c - is the light velocity in vacuum and λ - is the wavelength of light. For molecular maximum absorption spectrum, E can be responded by the molecular orbital energy level difference (ΔE), thus the photo absorption equation is replaced by the equation of $\Delta E = hc / \lambda$ is corresponds to the photon energy formula.

Based on the above photo absorption theory, the frontier molecular orbitals (FMOs) of the molecule have been investigated according to the results obtained from the B3LYP/6-311++G (d, p) calculations. The visible band observed around 232.99 nm could be attributed to high delocalization of π -electrons. These bands may be due to electronic transition of $\pi \rightarrow \pi^*$. The calculated UV-Vis spectrum is shown in Fig. 11 and values are represented in Table 11.

4.7. Molecular Electrostatic Potential (MESP)

Molecular Electrostatic Potential (ESP) surface vs. optimized electronic structure of HDP, intended for predicting hasty sites of the molecules by using the B3LYP/6-311++G(d,P) basis set with the computer software Molekel. To comprehend the qualified polarity of the molecules through the visual technique, to understand the association among the molecular structures as well as the physiochemical properties. The electrostatic potential is significant based on the effect of one molecule by another used for medicine-receptor and enzyme-substrate interactions. In the MEP, generated a charge distribution map around the molecule, which is exceedingly useful in accepting the reactive sites for nucleophilic and electrophilic attack in studies of biological identification and hydrogen bonding interactions. The province among red color is regarded as most electronegative (electrophilic) province and the province with blue colour is most positive (nucleophilic) region, whereas the bluish green color surrounded by the ring system of HDP is related to less positive region. The electrophilic and nucleophilic have red and blue colour respectively. Red colour is regarded as most electronegative region and blue colour is most positive region. For the zero regions represent the colour of green. This Figure provides a visual representation of the chemically active sites and comparative reactivity of atoms. Figs.12-14 represents ESP of zero and various applied electric fields. The ESP maps clearly emphasize the interactions and also highlight the difference in nature of interactions [28,29].

4.8. Temperature Dependence of Thermodynamic Properties

The temperature dependence of the thermodynamic properties namely, heat capacity at constant pressure (C_p), heat capacity (C_v), entropy (S), internal heat (U) Gibb's free energy (G) and enthalpy change (H) for the compounds HDP were determined by B3LYP/6-311++G(d,p) level and were listed in Table 12. Fig 15 depicts the correlation of heat capacity at constant pressure (C_p), Gibb's free energy (G), entropy (S) with temperature by B3LYP/6-311++G(d,p)

level. Table 12 reveals that the entropies, heat capacities, constant pressure, internal heat Gibb's free energy and enthalpy changes are increasing with temperature ranging from 10 to 500 K due to the fact that the molecular vibrational intensity increases with temperature [30]. The regression factors (R_2) of these observed relations of the thermodynamic functions vs. temperatures are all not less than 0.999. For the thermal energy, the regression coefficient (R_2) is 0.987. The correlation equations for the thermodynamic parameters with temperature are given in the graphs. These equations are used to predict the value of any thermodynamic parameters for any temperature.

$$S_m^0 = 43.67 + 0.394 T - 0.7 \times 10^{-4} T^2 \quad (R^2 = 0.99954) \quad (6-1)$$

$$C_{p,m}^0 = 1.401 + 0.301 T - 0.7 \times 10^{-4} T^2 \quad (R^2 = 0.99948) \quad (6-2)$$

$$H_m^0 = -43.58 + 0.0129T + 0.7 \times 10^{-4} T^2 \quad (R^2 = 0.99953) \quad (6-3)$$

4.9. Atomic Charges

Atomic charges for molecule can be derived in multiple ways with a high level of convergence to the same values and only then, knowing the remaining uncertainty, are suited for molecular simulations. Mulliken charges arise from the mulliken population analysis [31,32] and provide a means of estimating partial atomic charges from calculations carried out by the methods of computational chemistry. Generally, Mulliken population analysis (MPA) and Natural Population analysis (NPA) methods are used to calculate the atomic charges of atoms in molecules. The difference of MPA charges distribution for B3LYP/6-311+G (d,p) and B3LYP/6-311++G (d,p) are listed in Table 13. When the charge value decreases for C-atom the variations in MPA charge are small due to be systematic and almost uniform.

4.10. Mulliken Population Analysis

The Fukui function, $f(\vec{r})$ was introduced by Parr and Yang as the derivative of the chemical potential (μ) with respect to the external potential or equivalently as the derivative of the total electron density $\rho(\vec{r})$ upon a change in the total number of electrons.

$$f(\vec{r}) = \left(\frac{\delta\mu}{\delta v(\vec{r})} \right)_N = \left(\frac{\partial\rho(\vec{r})}{\partial N} \right)_{v(\vec{r})} \quad (7)$$

Due to the discontinuity of the derivative on the right-hand of equation at an integer value of N , three $f(\vec{r})$ can be defined at the point \vec{r} : $f^+(\vec{r})$, $f^-(\vec{r})$ and $f^0(\vec{r})$ which govern the nucleophilic, electrophilic and radical attacks, respectively. These functions can be condensed on atoms or functional groups k . In this sense, a scheme based on the finite difference approximation and population analysis was proposed by Yang and Moritier [33]

$$\begin{aligned} f_k^+ &\approx [N_k(N+1) - N_k(N)] \text{ governing nucleophilic attack} \\ f_k^- &\approx [N_k(N) - N_k(N-1)] \text{ governing electrophilic attack} \\ f_k^0 &\approx \frac{1}{2} [N_k(N+1) - N_k(N-1)] \text{ governing radical attack} \end{aligned}$$

Where N_k is the electronic population on site k for the systems with $(N-1)$, (N) and $(N+1)$ electrons evaluated at the same geometry with N -electron system. Using the well known finite difference approximation, dual descriptor $\Delta f(\vec{r})$ can be written as the difference between nucleophilic and electrophilic Fukui functions.

$$\Delta f(\vec{r}) \approx f^+(\vec{r}) - f^-(\vec{r}) \quad (8)$$

Equation (8) nicely shows why the dual descriptor allows identifying simultaneously the nucleophilic and electrophilic regions within a molecule. $\Delta f(\vec{r}) > 0$ at the point \vec{r} implies that the site is more favorable for a nucleophilic attack, whereas for $\Delta f(\vec{r}) < 0$ the electrophilic attack

is favored. Therefore, positive values of Δf_k define electrophilic regions within a molecular system whereas negative values will define the nucleophilic regions and a favorable chemical event occurs when electron accepting regions ($\Delta f(\vec{r}) > 0$) are aligned with electron donating regions ($\Delta f(\vec{r}) < 0$). Fukui functions, $f^-(\vec{r})$ and $f^+(\vec{r})$, carry information on the tendency for electronic rearrangement in those regions in the case of the electrophilic attack or nucleophilic attack. Mulliken population analysis calculated at $N_k(N+1)$, $N_k(N-1)$, $N_k(N)$ displayed, fukui function f_k^+ , f_k^- , f_k^0 and dual descriptor (Δf_k) are given in Table.14. The correlation graphic of condensed fukui function are shown in Fig.16. The electron density based on local reactivity descriptors; hardness, softness and the fukui function are proposed to explain the chemical selectivity or reactivity at a particular site of a chemical system. It has also been shown that local hardness is a reliable intermolecular reactivity descriptor and the local softness and fukui function are more reliable intramolecular site selectivity descriptors.

5. Conclusion

The crystals dimension of $8 \times 4 \times 2 \text{ mm}^3$ was grown by slow cooling method. The HRXRD study indicates that the grown crystal has a very low angle boundary. NMR study confirms the placement of protons in HDP molecule. FT-IR and FT-Raman spectra revealed the presence of various functional groups. The UV-Visible spectrum of HDP showed that the crystal is transparent in the range 300 – 1000 nm. Fluorescence spectrum shows that HDP fluoresces. We also carried out the density functional theory (DFT) calculations on the structure and vibrational spectra of HDP. The vibrational frequency analysis by B3LYP level agrees satisfactorily with experimental results. On the basis of agreement between the calculated and experimental results, assignments of all the fundamental vibrational modes of HDP were examined and proposed. Therefore, the assignments made at a higher level of the theory with higher basis set with

reasonable deviations from the experimental values, seems to be correct. HOMO and LUMO energy gap explains the eventual charge transfer interactions taking place within the compound. NLO property has also been observed by predicting the hyperpolarizability for the title compound due to the substitution in the benzene. MEP study shows that the electrophilic attack takes place at the C₅ position of HDP compound. Thermodynamic properties in the range from 10 to 500 K are obtained. Fukui indices are determining the local reactive site for the molecular systems during electrophilic, nucleophilic, radical and dual descriptor attacks. Over all, these results clearly show the superiority of MPA scheme. This study may be useful to design new efficient molecules with more electrical conductivity.

References

- [1] G. Velmurugan, S. Angeline Vedha, P. Venuvanalingam, RSC Adv. 4 (2014) 53060-53071.
- [2] K. Karuppasamy, R. Antony, Alwin, S. Balakumar, S, Sahaya Shajan, Materials Science Forum, 807 (2015) 41-63.
- [3] N. Nagarajan, G. Velmurugan, A. Prakash, N. Shakti, M. Katiyar, P. Venuvanalingam, R. Renganathan, Chem. Asian J. 9 (2014) 294-304.
- [4] Heng-guo Wang Shuang Yuan, Zhenjun Si, Xin-bo Zhang , Energy Environ. Sci., 2015,8, 3160-3165.
- [5] Aamer Saeed, Ifzan Arshad, Ulrich Flörke' J Chem, Volume 2013 (2013), Article ID 648121, 5 pages, <http://dx.doi.org/10.1155/2013/648121>.
- [6] D. Majumdar, J Chem Chem Sci, 5(12), (2105) 749-759.
- [7] G. Velmurugan, R. Jagadeesan, P. Venuvanalingam, RSC Adv. 6 (2015) 44569-44577.
- [8] R. Antony, S.T.D. Manickam, K. Karuppasamy, P. Kollu, P.V. Chandrasekar, . RSC Adv, 4 (2014) 42816-42824.
- [9] K. Lal, G. Bhagavannarayana, J. Appl. Cryst. 22 (1989) 209-215.

- [10] G. Bhagavannarayana, R.V. Ananthamurthy, G.C. Budakoti, B. Kumar, K.S.Bartwal, J. Appl. Cryst. 38 (2005) 768-771.
- [11] Hobart H. Willard, Lynne L. Merritt jr., John A. Dean, Frank A. Settle jr., Instrumental Methods of Analysis, Sixth Edition, Wadsworth Publishing Company. USA, 1986 pp.609.
- [12] M. J. Frisch. G. W. Trucks, H.B Schlegel et al., GAUSSIAN 09, Revision A.02, Gaussian, Inc., Wallingford CT, 2009.
- [13] T. Sundius, MOLVIB; A program for harmonic force field calculations, QCPE Program no. 604, J. Mol. Structure 218 (1990) 321-326.
- [14] T. Sundius, Vib. Spectrosc. 29 (2002) 89-94.
- [15] P. L. Polavara pu, J. Phys. Chem. 94(21), (1990), 8106-8112.
- [16] G. Keresztury, S. Holly, J. Varga, G. Besenyi, A. V. Wang, J. R. Durig, Spectrochim. Acta 49A (1993) 2007-2026.
- [17] G. Keresztury, J. M. Chalmers, P. R. Griffiths (Eds.), Raman spectroscopy Theory, Handbook of vibrational spectroscopy, Vol.1, John Wiley and sons Ltd., 2002, 71.
- [18] P. Pulay, G. Fogarasi, G. Pongar J.E. Boggs and A. Vargha, J Amer Chem Soc, 105 (1983) 7073-7079.
- [19] G. Fogarasi, X. Zhou, P.W. Jaylor and P. Pulay, J. Am. Chem. Soc., 114 (1992) 819-823.
- [20] D. Cecily Mary Glory, R. Madivanane and K. Sambathkumar Elixir Comp. Chem. 89 (2015) 36730-36741.
- [21] R. Rakhi, C.H. Suresh, Phys. Chem. Chem. Phys., 18 (2016) 24631-24641.
- [22] C. Sengamalai, M. Arivazhagan and K. Sampathkumar Elixir Comp. Chem. 56 (2013) 13291-13298.
- [23] K Sambathkumar, S Nithiyantham, J Mater Sci: Mater Electron, 28 (2017) 6529-6543
- [24] S. Yusuf, U. Fatih, A. Gamal, E. Hiti, K. Smith, S. Amany, Hegazy J Spectroscopy doi.org/10.1155/2016/5396439(2016).

- [25] R. Ditchfield, *J. Chem. Phys.* 56 (1972) 5688–5691.
- [26] Y. Ataly, D. Avai, A. Basoglu, *Struct. Chem.* 19 (2008) 239–246.
- [27] T. Vijayakumar, I. Hubert Joe, C.P.R. Nair, V.S. Jayakumar, *Chem. Phys.* 343 (2008) 83–99.
- [28] K. Sambathkumar, *Elixir Vib.Spec.* 91 (2016) 38381-38391.
- [29] K.Smbathkumar *Spectrochim. Acta A*, 147 (2015) 51-66.
- [30] B. Latha, P. Kumaresan, S. Nithiyantham, K. Sambathkumar, *J. Mol. Struct.* 1142 (2017) 255-260.
- [31] I.G. Csizmadia, *Theory and Practice of MO Calculations on Organic Molecules*, Elsevier, Amsterdam, 1976.
- [32] C. Morell, A. Grand, A. Toro-Labbe, *Chem. Phys. Lett.*, 425 (2006) 342-348.
- [33] R.S. Mulliken, “Electronic Population Analysis On - Mo Molecular Wave Functions, *J. Chem., Phys.*, 23, (1995) 1833-1839.
- [34] Muhammad Nadeem Arshad , Aisha Bibi , Tariq Mahmood , Abdullah M. Asiri, Khurshid Ayub, *Molecules* 20, (2015) 5851-5874.

Table 1. Crystal data and structure refinement for the Hydrazine (1,3- dinitrophenyl)

Molecular formula	C ₆ H ₆ N ₄ O ₄
Formula weight	153.20
Temperature	295(2)K
Wavelength	0.71073 Å
Crystal system	Monoclinic
Space group	'P 21/c'
Unit cell dimensions	
a	4.819(3)Å ^o
b	11.625(4)Å ^o
c	14.268(4)Å ^o
α	90 ^o
β	97.04(4) ^o
γ	90 ^o
Volume	793.28 cm ³
Z	4
Calculated density	1.403 g/m ³
Absorption correction	None
F(000)	208
Crystal size	0.3x0.2x0.18mm
Completeness to theta=30.05 ^o	100.0%
Theta rang for data collection	1.53-30.05 ^o
Refinement method	Full-matrix least-squares on F ²
R indices (all data)	R ₁ = 0.04, wR ₂ = 0.04

Table 2. Atomic coordinates and equivalent parameters ($\text{Å}^2 \times 10^3$) of Hydrazine (1,3-dinitrophenyl)

Atom	x	y	z
O1	0.5646(9)	0.0172(4)	0.6910(3)
O2	0.2348(8)	0.1200(3)	0.7365(3)
O3	0.9543(8)	0.1006(4)	0.4081(3)
O4	0.7937(9)	0.2435(4)	0.3210(3)
N1	0.115(1)	0.3226(4)	0.6617(3)
N2	0.014(1)	0.4309(5)	0.6513(4)
N3	0.411(1)	0.1011(4)	0.6822(3)
N4	0.804(1)	0.1853(5)	0.3928(3)
C1	0.281(1)	0.2869(4)	0.5981(3)
C2	0.431(1)	0.1812(5)	0.6061(3)
C3	0.604(1)	0.1493(5)	0.5395(4)
C4	0.628(1)	0.2195(5)	0.4642(4)
C5	0.480(1)	0.3217(5)	0.4529(4)
C6	0.314(1)	0.3553(5)	0.5182(4)
H1	0.10(1)	0.275(5)	0.708(4)
H2	0.04(1)	0.478(5)	0.701(4)
H3	-0.19(1)	0.417(5)	0.660(4)
H4	0.701(8)	0.081(4)	0.544(3)
H5	0.51(1)	0.371(5)	0.405(4)
H6	0.23(1)	0.423(4)	0.516(3)

Table 3. Optimized geometrical parameters of Hydrazine (1,3- dinitrophenyl) by B3LYP /6-311+G(d,p) and B3LYP/6-311++G(d,p) level.

Bond Length	Value (Å)			Bond Angle	Value (°)			Dihedral Angle	Value (°)		Exp
	B3LYP/6-311+G(d,p)	B3LYP/6-311++G(d,p)	Exp		B3LYP/6-311+G(d,p)	B3LYP/6-311++G(d,p)	Exp		B3LYP /6-311 + G(d,p)	B3LYP/6-311++ (d,p)	
R(1,2)	1.3899	1.3996	1.500(3)	A(2,1,6)	104.6367	104.9363	116.71(16)	D(6,1,2,3)	-0.3412	-1.3412	
R(1,6)	1.3141	1.3242		A(2,1,7)	127.571	128.5710		D(6,1,2,10)	176.657	179.657	
R(1,7)	1.4682	1.4985	1.391(3)	A(6,1,7)	120.7922	123.7922		D(7,1,2,3)	173.7271	179.7271	
R(2,3)	1.4221	1.4721	1.400(3)	A(1,2,3)	117.2705	119.2705	116.22(16)	D(7,1,2,10)	-0.2747	-0.9747	
R(2,10)	1.0750	1.2070		A(1,2,10)	120.4123	121.4123		D(2,1,6,5)	0.7868	0.9868	
R(3,4)	1.4329	1.4729	1.389(3)	A(3,2,10)	120.3172	120.9172		D(7,1,6,5)	-176.2818	-179.2818	
R(3,11)	1.4789	1.5729		A(2,3,4)	122.0802	124.0802		D(2,1,7,8)	-144.079	-149.079	
R(4,5)	1.3561	1.3990	1.387(3)	A(2,3,11)	118.0157	119.0157		D(2,1,7,9)	88.8107	90.8107	
R(4,14)	1.1686	1.2486		A(4,3,11)	116.9039	117.9039		D(6,1,7,8)	31.0047	33.0047	
R(5,6)	1.3242	1.3742	1.383(3)	A(3,4,5)	115.3840	117.3840	121.19(17)	D(6,1,7,9)	-85.1057	-89.1057	
R(5,15)	1.4690	1.4891	1.352(2)	A(3,4,14)	121.3215	121.9215		D(1,2,3,4)	0.0735	1.0735	
R(7,8)	1.3317	1.3687	1.234(2)	A(5,4,14)	120.2944	120.9944		D(1,2,3,11)	177.9376	179.9376	
R(7,9)	1.3599	1.3899	1.232(2)	A(4,5,6)	102.494	104.494	119.81(18)	D(10,2,3,4)	-174.9247	-179.9247	
R(11,12)	1.3612	1.3812	1.229(2)	A(4,5,15)	123.554	125.554		D(10,2,3,11)	-0.0605	-0.9605	
R(11,13)	1.3595	1.3895	1.235(2)	A(6,5,15)	126.9517	127.9517		D(2,3,4,5)	0.1689	0.8689	
R(15,16)	1.1003	1.1103		A(1,6,5)	122.1322	123.1322	120.37(18)	D(2,3,4,14)	-177.827	-179.827	

R(15,17)	1.4015	1.4415	1.391(2)	A(1,7,8)	108.8017	109.8017	123.32(18)	D(11,3,4,5)	-178.6954	-179.6954
R(17,18)	1.1213	1.1876		A(1,7,9)	109.4849	110.4849	122.54(16)	D(11,3,4,14)	0.3087	1.3087
R(17,19)	0.9374	0.9979		A(8,7,9)	109.3886	109.8886		D(2,3,11,12)	-90.3121	-91.3121
				A(3,11,12)	108.3011	109.3011	118.28(17)	D(2,3,11,13)	145.8428	148.8428
				A(3,11,13)	109.4612	110.96 12	118.73(15)	D(4,3,11,12)	85.5606	88.5606
				A(12,11,13)	107.4351	109.4351		D(4,3,11,13)	-30.2846	-31.2846
				A(5,15,16)	106.6601	109.6601	118.71(16)	D(3,4,5,6)	-0.0613	-0.9613
				A(5,15,17)	108.8305	109.8305	119.93(16)	D(3,4,5,15)	178.7402	179.9402
				A(16,15,17)	105.0571	107.0571		D(14,4,5,6)	178.0347	179.9347
				A(15,17,18)	109.2167	109.9167		D(14,4,5,15)	-0.2638	-0.8638
				A(15,17,19)	109.2685	110.2685	121.42(17)	D(4,5,6,1)	-0.0612	-0.5612
				A(18,17,19)	106.9046	109.9046	117.22(16)	D(15,5,6,1)	179.0383	179.6383

^aFor numbering of atoms refer Fig. 5

^aExperimental values are taken from Ref.[41].

Table 4. Definition of internal coordinates of Hydrazine (1,3- dinitrophenyl).

No. (i)	Symbol	Type	Definition
1-3	Ri	C-N	C2-N7,C4-N11,C5-N14
4-6	ri	C-H	C3-H10,C1-H20,C6-H19
7	Si	N-H	N14-H15
8,9	qi	N-H ₂	N16-H17,N16-H18
10	Qi	N-N	N14-N16
11-16	Pi	C-C	C1-C2,C2-C3,C3-C4,C4-C5,C5-C6,C6-C1
17-20	Si	N-O	N2-O9,N7-O8,N11-O12,N11-O13
In-plane bending			
21-26	α_i	ring	C1-C2-C3,C2-C3-C4,C3-C4-C5,C4-C5-C6,C5-C6-C1,C6-C1-C2
27-32	β_i	CCH	C2-C3-H10,C4-C3H10,C5-C6-H19,C1-C6-H19,C2-C1-H20,C6-C1-H20
33-36	γ_i	CNO ₂	C2-N7-O8,C2-N7-O9,C4-N11-O12,C4-N11-O13
37-38	θ_i	ONO	O8-N7-O9,O12-N11-O13
39-40	ϕ_i	NNH ₂	N14-N16-H17,N14-N16-H18
41	π_i	HNH	H17-N16-H18
42	σ_i	NNH	N16-N14-H15
43-48	ω_i	CCN	C5-C4-N11,C3-C4-N11,C1-C2-N7,C3-C2-N7,C6-C5-N14,C4-C5-N14
49	λ_i	NHC	H15-N14-C5
Out-of-plane bending			
50-52	ψ_i	HC	H20-C1-C2-C6,H10-C3-C4-C2,H19-C6-C5-C1
53	δ_i	NN	N16-N14-H15-C5
54	η_i	NH	H15-N14-C5-N16
55-57	χ_i	CN	N7-C2-C1-C3,N11-C4-C3-C5,N14-C5-C6-C4
Torsion			
58-63	τ_i	ring	C1-C2-C3-C4,C2-C3-C4-C5,C3-C4-C5-C6,C4-C5-C6-C1,C5-C6-C1-C2,C6-C1-C2-C3
64	τ_i	tNH ₂	N14-N16-H17-H18
65-66	τ_i	tNO ₂	C2-N7-O9-O8,C4-N11-O12-O13

^aFor numbering of atoms refer Fig.5

Table 5 Definition of local symmetry coordinates of Hydrazine (1,3- dinitrophenyl)

No. (1)	Type ^a	Definition
1-3	C-N	R_1, R_2, R_3
4-6	C-H	r_4, r_5, r_6
7	N-H	S_7
8	NH _{2SS}	$q_8 + q_9 / \sqrt{2}$
9	NH _{2ass}	$q_8 - q_9 / \sqrt{2}$
10	N-N	Q_{10}
11-16	C-C	$P_{11}, P_{12}, P_{13}, P_{14}, P_{15}, P_{16}$
17,18	NO _{2 SS}	$S_{17+} S_{18} / \sqrt{2}, S_{19+} S_{20} / \sqrt{2}$
19,20	NO _{2 ass}	$S_{17-} S_{18} / \sqrt{2}, S_{19-} S_{20} / \sqrt{2}$
21	R trigd	$(\alpha_{21} - \alpha_{22} + \alpha_{23} - \alpha_{24} + \alpha_{25} - \alpha_{26}) / \sqrt{6}$
22	R symd	$(-\alpha_{21} - \alpha_{22} + 2\alpha_{23} - \alpha_{24} - \alpha_{25} + 2\alpha_{26}) / \sqrt{12}$
23	R asymd	$(\alpha_{21} - \alpha_{22} + \alpha_{25} - \alpha_{26}) / 2$
24-26	bCH	$(\beta_{27} - \beta_{28}) / \sqrt{2}, (\beta_{29} - \beta_{30}) / \sqrt{2}, (\beta_{31} - \beta_{32}) / \sqrt{2}$
27,28	NH _{2rock}	$(\gamma_{33} - \gamma_{34}) / \sqrt{2}, (\gamma_{35} - \gamma_{36}) / \sqrt{2}$
29,30	NH _{2twist}	$(\gamma_{33} - \gamma_{34}) / \sqrt{2}, (\gamma_{35} - \gamma_{36}) / \sqrt{2}$
31,32	NH _{2symm}	$(2\gamma_{37} - \gamma_{33} - \gamma_{34}) / \sqrt{2}, (2\gamma_{38} - \gamma_{35} - \gamma_{36}) / \sqrt{2}$
33	NH _{2rock}	$(\phi_{39} - \phi_{40}) / \sqrt{2}$
34	NH _{2twist}	$(\phi_{39+} \phi_{40}) / \sqrt{2}$
35	NH _{2sciss}	$(2\pi_{41} - \phi_{39} - \phi_{40}) / \sqrt{2}$
36	bHNNH	$(\sigma_{42} / \sqrt{2})$
37-39	bCCN	$\omega_{43-} \omega_{44} / \sqrt{2}, \omega_{45-} \omega_{46} / \sqrt{2}, \omega_{47-} \omega_{48} / \sqrt{2},$
40	bNCH	$(\lambda_{49} / \sqrt{2})$
41-43	ψ HC	$\Psi_{50}, \Psi_{51}, \Psi_{52}$
44	δ NN	δ_{53}
45	η NH	η_{54}
46-48	χ CN	$\chi_{55}, \chi_{56}, \chi_{57}$
49	t R trigd	$(\tau_{58} - \tau_{59} + \tau_{60} - \tau_{61} + \tau_{62} - \tau_{63}) / \sqrt{6}$
50	t R symd	$(\tau_{58} - \tau_{59} + \tau_{61} - \tau_{63}) / 2$
51	t R asymd	$(-\tau_{58} + 2\tau_{59} - \tau_{60} - \tau_{61} + 2\tau_{62} - \tau_{63}) / \sqrt{12}$
52	tNH ₂	τ_{64}
53,54	tNO ₂	τ_{65}, τ_{66}

^aThese symbols are used for description of normal modes by TED in Table 7.

Table 6. Optimized global minimum energies of different conformers of Hydrazine (1,3-dinitrophenyl) calculated at B3LYP/6-311+G(d,p) and B3LYP/6-311++G(d,p) level of theory.

Conformer	Optimized global minimum energies (in Hartrees)	
	B3LYP/6-311+G(d,p)	B3LYP/6-311++G(d,p)
A	-750.2035	-750.2166
B	-750.2136	-750.2369
C	-750.2094	-750.2967*
D	-750.1085	-750.2261

*Global minimum energy

Table 7: The observed (FTIR and FT-Raman) and calculated (unscaled and scaled) fundamental harmonic frequencies (cm^{-1}), force constant (mdyn A^{-1}), infrared-intensity (km/mol), Raman activity (\AA amu^{-1}) and probable assignments of Hydrazine (1,3-dinitrophenyl) are analyzed based on SQM force field calculation using B3LYP/6-311+G(d,p) and B3LYP/6-311++G(d,p) level.

Observed frequencies		B3LYP/6-311+G(d,p)					B3LYP/6-311++G(d,p)					Assignments (TED %)
FTIR	FT-Raman	Calculated Frequency		Force Const	IR intensity	Raman activity	Calculated Frequency		Force Const	IR intensity	Raman activity	
		Unscaled	Scaled				Unscaled	Scaled				
3312vw		3658	3302	7.7223	2.1489	289.998	3698	3313	9.2144	91.363	175.04	NH2ass(99)
3228vs		3541	3212	8.1355	34.411	138.802	3571	3229	8.8809	39.404	71.173	NH2ss(98)
	3176vw	3529	3170	8.8210	7.4872	127.275	3559	3175	7.8310	45.707	165.01	vNH(96)
3144s		3253	3120	2.0700	41.957	39.109	3283	3142	6.5937	2.0800	84.324	vCH(88) vCC(12)
3098s		3214	3088	6.8862	17.936	47.985	3274	3099	6.5873	4.0972	117.00	vCH(86) vCC(11)
3077ms		3209	3067	6.9356	32.625	34.766	3259	3078	6.4606	3.8158	47.117	vCH(85) vCC(10)
1699w		1969	1680	2.9517	110.87	2.2458	1999	1697	6.3934	15.974	108.38	vCC(83) vNH(12)
1687vw		1942	1676	5.2220	21.034	28.5009	1982	1685	9.5105	145.02	219.55	vCC(84) vCH(13)
	1679vw	1889	1662	9.7922	73.120	9.956	1899	1676	2.1445	160.79	4.4309	vCC(82) vCH(11)
	1670vw	1867	1655	8.6932	237.53	4.0862	1890	1673	6.1090	73.396	44.788	vCC(80) vCH(15)
1664vw		1858	1649	8.1760	54.067	0.8294	1879	1668	3.6920	53.834	43.119	vCC(51),vCN(11),bNH(10)
1651vw		1845	1634	9.4856	58.504	9.0907	1866	1655	3.7490	17.087	5.5291	vCC(46),vCN(25),bCH(14)
1646vw		1819	1625	3.4425	31.942	90.173	1845	1642	3.4063	26.583	2.5886	NO ₂ ass(77),vCC(10)
1635vw		1806	1612	5.1888	61.040	23.683	1826	1634	30758	112.41	150.53	NO ₂ ass(76),vCC(16)
1628w		1788	1601	7.2713	8.5719	19.312	1791	1629	1.9855	146.71	118.78	NH2siss(75),NO ₂ ass(17)
1619w		1779	1592	13.645	379.81	74.288	1787	1621	2.7027	107.84	50.713	NO ₂ ss(74),NH2siss(14)
1610vw		1765	1580	1.1453	0.1253	5.5749	1776	1613	3.8289	184.09	34.092	NO ₂ ss(73),NO ₂ twist(19)
	1593s	1755	1571	8.7552	64.489	254.28	1761	1595	0.9625	8.4852	16.216	vCN(48),vNN(29), bCH(10)
1589vs		1743	1560	36.965	1.0509	964.80	1753	1588	1.1284	224.07	11.982	vCN(42),bNH(21), bCH(16)
	1574s	1736	1551	6.3548	2.4291	984.05	1745	1575	1.5659	14.384	50.743	vCN(67), bNH(33)
1576s		1724	1547	6.4462	2.0954	1006.1	1731	1577	1.2113	33.860	19.420	vNN(51),bCH(22),Rasynd(13)
1554vs		1706	1540	0.8197	51.603	1.0699	1719	1555	1.6561	0.6344	0.7102	bNH(49),bCH(23),Rasynd(17)
	1496w	1698	1484	3.6457	6.3828	18.755	1701	1497	0.7618	3.0499	0.3020	bCH (47),NH ₂ rock(28),vCN(12)
1392s		1678	1381	4.5807	8.4919	27.651	1689	1393	0.7304	0.5211	0.4702	bCH(46),Rasynd(21),vCN(18)
	1373s	1652	1364	4.8339	15.106	9.3577	1671	1374	1.3233	44.251	27.121	bCH(45),Rasynd(25),vCN(12)
	1278vs	1634	1261	5.6570	13.090	5.1159	1663	1279	0.7310	55.676	0.2925	NH ₂ rock(56) Rtrigd(61), ω NH(18)
	1262s	1618	1255	0.7593	0.8925	2.8779	1653	1263	2.3645	7.6061	60.737	Rasynd(65),NH ₂ wag(25)
1250vs		1603	1241	1.2875	17.655	0.7286	1636	1252	0.5021	5.5053	3.8313	Rasynd(67), ω NH(29)

1240s		1578	1233	3.9544	41.736	0.3190	1599	1239	1.3648	0.1684	6.3140	Rtrigd(64), ω NH(31)
	1212w	1567	1202	3.5802	2.2215	2.4389	1587	1213	1.6858	6.9489	7.4030	NH2wag(65),bNN(23)
	1190w	1544	1180	0.2377	57.325	4.0707	1563	1191	1.6848	5.9706	11.051	ω NH(51), ω CH (47)
1003s		1523	993	1.3033	2.6818	1.1251	1554	1004	1.1149	5.9332	2.3820	ω CH(62),Rsymd(28)
	991s	1516	986	1.6843	26.910	0.8863	1523	992	0.2284	8.2217	5.8321	ω CH(63),Rtrigd(33)
	987vw	1509	978	1.4663	11.600	0.6538	1517	988	0.4504	13.134	1.3548	bNN(48),bCN(44)
975w		1478	969	0.8175	12.969	0.6840	1484	976	0.7134	12.041	2.9926	ω CH (47),bNN(28)
966w		1456	958	1.5050	15.007	2.8833	1470	965	0.4801	10.543	1.2167	bCN(64),NO2sciss(17)
	952vw	1298	947	0.9082	0.6119	8.2751	1312	953	0.3172	1.3856	1.4217	bCN(66),NO2sciss(31)
944w		1267	931	0.1767	253.04	4.3170	1296	945	0.3618	13.651	1.4167	bCN(54), ω CH(27)
931w		1234	925	0.9024	1.3415	2.2996	1287	933	0.1033	159.57	4.6727	NO2sciss(61), ω CH(21)
	927w	1223	912	0.0799	121.18	0.6237	1266	929	0.0792	114.34	1.8745	NO2sciss(61), ω CH(29)
912ms		1209	906	0.8641	2.3905	4.3467	1249	913	0.2798	5.1609	1.7402	NO2wag(64), ω CH(26)
	841w	1191	830	0.7142	0.1962	5.5151	1219	845	0.2336	0.4261	0.7323	NO2wag(55), ω CH(25)
791w		1167	787	0.0985	8.1796	1.5888	1209	794	0.1364	5.9234	1.9773	tRtrigd(59),NO2wag(30)
763w		1145	756	0.1777	2.8972	1.6502	1175	762	0.0341	20.075	0.7223	tRsymd(53),NH2wag(21)
610w		1134	604	0.3821	2.5352	1.5602	1164	612	0.0111	5.2422	4.1975	tRasymd(48),bNN(29)
	494w	1122	489	0.1404	5.3971	0.3441	1142	495	5.9706	0.1962	2.4389	NO2rock(56),NO2wag(34)
	487w	1109	478	0.0710	6.4649	0.3712	1129	489	5.9332	8.1796	4.0707	NO2rock(58),NO2sciss(35)
476w		1001	466	0.0763	1.9786	1.1324	1019	477	8.2217	2.8972	1.1251	ω CN(51),NO2sciss(41)
451w		990	441	0.0241	0.4590	1.4314	999	452	13.134	2.5352	0.8863	ω CN(50), ω CH(49)
432w	431w	876	422	0.0290	0.5825	1.5831	893	433	12.041	5.3971	0.6538	ω CN(57), ω CH(34)
421s		834	401	0.0230	0.2009	0.1699	854	424	6.9706	6.4649	0.6840	ω NN(52), ω CH(43)
412w		756	399	8.8809	39.404	71.173	766	414	6.354	2.4291	984.05	NO2twist(51)
	342w	666	330	7.8310	45.707	165.01	689	345	6.446	2.0954	1006.1	NO2twist(49)
	284w	645	264	6.5937	2.0800	84.324	675	286	0.819	51.603	1.0699	NH2twist(42)

Abbreviations: v - stretching; b - in-plane bending; ω - out-of-plane bending; asymd - asymmetric; symd - symmetric; t - torsion; trig - trigonal; w - weak; vw-very weak; vs - very strong; s - strong; ms - medium strong; ss - symmetric stretching; ass - asymmetric stretching; ips - in-plane stretching; ops - out-of-plane stretching; sb - symmetric bending; ipr - in-plane rocking; opr - out-of-plane rocking; opb - out-of-plane bending.

Table 8. Calculated Nonlinear optical properties of Hydrazine (1,3-dinitrophenyl) at B3LYP/6-311++G(d,p) level.

NLO behavior	Value
Optimized global minimum Energy	-470768(Kcal/mol)
Dipole moment (μ)	2.88 Debye
Mean polarizability (α)	1.0649×10^{-30} esu
Anisotropy of the polarizability ($\Delta\alpha$)	3.7496×10^{-30} esu
First hyperpolarizability (β)	0.4234×10^{-30} esu
Vector-first hyperpolarizability (β_{vec})	0.1740×10^{-30} esu

Table 9. Calculated HOMO-LUMO energy gap and related molecular properties of Hydrazine (1,3-dinitrophenyl).

Molecular Properties	B3LYP/6-311++G(d,p)
HOMO	-6.8533eV
LUMO	-3.3701eV
Energy gap	3.4885eV
Ionization Potential (I)	-6.8533eV
Electron affinity (A)	-3.3701eV
Global softness (s)	425.1859eV
Global Hardness (η)	-1.7415eV.
Chemical potential (μ)	-4.8573eV
Global Electrophilicity (ω)	-7.499eV
Inhibition efficiency through back donations	-0.2691

Table 10. The calculated shifts of carbon and hydrogen atoms of Hydrazine (1,3-dinitrophenyl) using B3LYP/6-311++G(d,p) GIAO method

Atom position	Theoretical 6-311++G(d,p)	Exp ^a	Δ
C1	118.009	187.473	69.464
C2	-172.158		
C3	162.033	123.56	-38.473
C4	31.7285	42.456	10.7275
C5	123.043	140.56	17.517
C6	76.798	82.734	5.936
H7	-34.8453		
N8	62.357	66.430	4.073
O9	137.53	153.671	16.141
O10	141.11	143.67	2.56
H11	21.66	25.635	3.975
N12	196.235	199.89	3.655
O13	105.87	88.45	-17.42
O14	103.83	81.32	-22.51
H15	24.089	22.678	-1.411
N16	155.99		
H17	28.191		
N18	198.993		
H19	34.950		
H20	38.595		

^a Taken from Ref [34] and $\Delta(\delta_{\text{exp}}-\delta_{\text{the}})$; difference between respective chemical shifts.

Table 11. The computed excitation energies, oscillator strength, electronic transition configuration wavelength of Hydrazine (1,3-dinitrophenyl) using TD-DFT/B3LYP/6-311++G(d,p) level.

Excited state	EE(ev)	Oscillator strength f	Configuration	CI expansion coefficient	Wavelength (nm)
1	4.2383	0.0832	38 → 40	0.56650	382.86
2	5.7606	0.8799	39 → 41	0.23463	390.11
			40 → 41	0.47912	
3	3.1648	0.5111	37 → 41	-0.59777	400.12
			38 → 41	0.45081	
4	5.3214	0.1314	37 → 41	-0.39904	435.99
			38 → 41	-0.31580	
5	6.1964	0.6727	39 → 42	0.45016	540.01
			40 → 42	-0.31512	
			40 → 47	-0.30668	
6	4.2450	0.4822	40 → 42	0.21565	781.23
			38 → 47	-0.27820	
			38 → 48	-0.20788	
			40 → 43	0.10296	

Table 12. Thermodynamic functions of Hydrazine (1,3-dinitrophenyl) determined at different temperatures with B3LYP/6-311++G(d,p) level.

Temperature (K)	C_v (J/K/mol)	C_p (J/K/mol)	U (kJ/mol)	H (kJ/mol)	S (J/K/mol)	G (kJ/mol)	Q	ln(Q)
10.000	24.944	33.258	61.456	61.539	162.323	59.916	5.51448E+06	15.5228
20.000	25.102	33.416	61.706	61.872	185.397	58.165	8.82568E+07	18.2957
30.000	26.028	34.342	61.961	62.211	199.094	56.238	4.48622E+08	19.9216
40.000	27.470	35.785	62.228	62.561	209.165	54.194	1.43618E+09	21.0852
50.000	29.103	37.418	62.511	62.927	217.322	52.061	3.58697E+09	22.0005
60.000	30.948	39.262	62.811	63.310	224.303	49.852	7.67820E+09	22.7616
80.000	35.404	43.719	63.473	64.138	236.186	45.243	2.64785E+10	23.9996
90.000	37.909	46.223	63.840	64.588	241.479	42.855	4.47787E+10	24.5250
100.000	40.478	48.792	64.232	65.063	246.482	40.415	7.25225E+10	25.0071
110.000	43.035	51.349	64.649	65.564	251.253	37.926	1.13498E+11	25.4550
120.000	45.529	53.843	65.092	66.090	255.828	35.390	1.72748E+11	25.8751
130.000	47.931	56.245	65.559	66.640	260.233	32.810	2.56927E+11	26.2720
140.000	50.229	58.544	66.050	67.214	264.486	30.186	3.74735E+11	26.6494
150.000	52.424	60.739	66.564	67.811	268.601	27.521	5.37463E+11	27.0101
160.000	54.522	62.837	67.098	68.429	272.588	24.815	7.59656E+11	27.3561
170.000	56.533	64.847	67.654	69.067	276.458	22.069	1.05993E+12	27.6892
180.000	58.465	66.779	68.229	69.725	280.220	19.286	1.46195E+12	28.0107
190.000	60.327	68.641	68.823	70.403	283.881	16.465	1.99568E+12	28.3220
200.000	62.127	70.441	69.435	71.098	287.448	13.609	2.69879E+12	28.6238
210.000	63.870	72.185	70.065	71.811	290.927	10.717	3.61847E+12	28.9170
220.000	65.561	73.876	70.712	72.542	294.324	7.790	4.81356E+12	29.2024
230.000	67.203	75.517	71.376	73.289	297.644	4.830	6.35706E+12	29.4805
240.000	68.797	77.111	72.056	74.052	300.892	1.838	8.33925E+12	29.7519
250.000	70.345	78.660	72.752	74.831	304.072	1.187	1.08713E+13	30.0171
260.000	71.849	80.163	73.463	75.625	307.186	4.244	1.40897E+13	30.2764
270.000	73.307	81.622	74.189	76.434	310.239	7.331	1.81611E+13	30.5303
280.000	74.721	83.036	74.929	77.257	313.233	10.448	2.32889E+13	30.7790
290.000	76.091	84.406	75.683	78.094	316.171	13.595	2.97200E+13	31.0228
300.000	77.418	85.732	76.451	78.945	319.055	16.771	3.77535E+13	31.2621
310.000	78.701	87.015	77.231	79.809	321.887	19.976	4.77504E+13	31.4970
320.000	79.940	88.255	78.025	80.685	324.669	23.209	6.01454E+13	31.7277
330.000	81.138	89.452	78.830	81.574	327.404	26.469	7.54605E+13	31.9546
340.000	82.293	90.608	79.647	82.474	330.091	29.757	9.43204E+13	32.1777
350.000	83.408	91.722	80.476	83.386	332.734	33.071	1.17472E+14	32.3972
360.000	84.482	92.796	81.315	84.308	335.333	36.411	1.45803E+14	32.6132
370.000	85.516	93.831	82.165	85.242	337.890	39.778	1.80371E+14	32.8260
380.000	86.513	94.827	83.025	86.185	340.405	43.169	2.22429E+14	33.0356
390.000	87.472	95.786	83.895	87.138	342.881	46.586	2.73457E+14	33.2421
400.000	88.395	96.709	84.775	88.101	345.318	50.027	3.35204E+14	33.4457
410.000	89.282	97.597	85.663	89.072	347.717	53.492	4.09729E+14	33.6465
420.000	90.136	98.451	86.560	90.052	350.079	56.981	4.99452E+14	33.8445
430.000	90.958	99.272	87.466	91.041	352.405	60.493	6.07208E+14	34.0398
440.000	91.748	100.062	88.379	92.038	354.697	64.029	7.36318E+14	34.2326
450.000	92.507	100.822	89.301	93.042	356.954	67.587	8.90660E+14	34.4229
460.000	93.238	101.552	90.229	94.054	359.178	71.168	1.07476E+15	34.6108
470.000	93.940	102.254	91.165	95.073	361.369	74.771	1.29386E+15	34.7964
480.000	94.616	102.930	92.108	96.099	363.529	78.395	1.55409E+15	34.9796
490.000	95.266	103.580	93.057	97.132	365.658	82.041	1.86253E+15	35.1607
500.000	95.891	104.206	94.013	98.171	367.757	85.708	2.22738E+15	35.3396

Table 13. Calculated Mulliken's Charges of Hydrazine (1,3-dinitrophenyl) at B3LYP/6-311+G (d,p) and B3LYP/6-311++G (d,p) level.

Atom No	B3LYP/6- 311+G (d,p)	B3LYP/6- 311++G (d,p)
C1	0.277126	0.401740
C2	-0.252946	-0.240653
C3	0.021987	-0.072572
C4	-1.111045	-0.490080
C5	-0.162810	-0.466483
C6	1.220702	0.828902
N7	-0.501957	-0.479224
O8	0.019083	-0.000239
O9	0.053180	0.051036
H10	0.308978	0.316782
N11	-0.499351	-0.446352
O12	0.015552	-0.015689
O13	0.052653	0.049273
H14	0.264636	0.268373
N15	-0.445352	-0.599714
H16	0.418521	0.373945
N17	-0.674461	-0.473866
H18	0.384224	0.311917
H19	0.371550	0.366567
H20	0.239730	0.316339

Table 14. Mulliken population analysis calculated at $N_k(N+1)$, $N_k(N-1)$, $N_k(N)$ and condensed Fukui function of Hydrazine (1,3-dinitrophenyl).

Atom No	$N_k(N+1)$	$N_k(N-1)$	$N_k(N)$	f_k^+	f_k^-	f_k^0
C1	-0.069555	-0.074432	0.277126	-0.346681	0.35155	0.00243
C2	0.004481	0.164462	-0.252946	0.257427	-0.417408	-0.07999
C3	-0.095904	-0.106795	0.021987	-0.117891	0.128782	0.00544
C4	0.295905	0.075350	-1.111045	1.40695	-1.186395	0.11027
C5	-0.067370	-0.065107	-0.162810	0.09544	-0.097703	-0.00113
C6	0.274316	0.229701	1.220702	-0.946386	0.991001	0.02230
N7	0.129574	0.007978	-0.501957	0.631531	-0.509935	0.06079
O8	0.072570	-0.016837	0.019083	0.053487	0.03592	0.04470
O9	0.143735	0.009768	0.053180	0.090555	0.043412	0.06698
H10	0.000680	-0.004995	0.308978	-0.308298	0.313973	0.00283
N11	0.131164	0.009574	-0.499351	0.631099	-0.508925	0.06079
O12	0.063776	-0.007802	0.015552	0.048224	0.023354	0.03578
O13	0.147674	-0.002605	0.052653	0.095021	0.055258	0.07513
H14	-0.014607	-0.004954	0.264636	-0.279243	0.26959	-0.00482
N15	-0.005019	0.427772	-0.445352	0.440333	-0.87312	-0.21639
H16	-0.000161	-0.017065	0.418521	-0.41868	0.435586	0.00845
N17	0.000365	0.415269	-0.674461	0.674826	-1.08973	-0.20745
H18	-0.000098	-0.016951	0.384224	-0.384322	0.401175	0.00842
H19	-0.000399	-0.016607	0.371550	-0.371949	0.388157	0.00810
H20	-0.011127	-0.005722	0.239730	-0.250857	0.24545	-0.00270